To the Graduate Council:

I am submitting herewith a thesis written by Melanie Jean Kirkham entitled "Investigation of a Phase Transition in Pure and Magnesia- and Titania-Substituted Hexacelsian." I have examined the final electronic copy of this thesis for form and content and recommend that it be accepted in partial fulfillment of the requirements for the degree of Master of Science, with a major in Materials Science and Engineering.

Claudia J. Rawn .
Major Professor

We have read this thesis
and recommend its acceptance:

Joseph E. Spruiell .

David C. Joy .

Theodore C. Labotka .

Accepted for the Council:

Anne Mayhew .
Vice Chancellor and
Dean of Graduate Studies

(Original signatures are on file with official student records.)

INVESTIGATION OF A PHASE TRANSITION IN PURE AND MAGNESIA- AND TITANIA-SUBSTITUTED HEXACELSIAN

A Thesis

Presented for the

Master of Science

Degree

The University of Tennessee, Knoxville

Melanie Jean Kirkham

May 2005

ACKNOWLEDGEMENTS

The author would like to thank Claudia J. Rawn for serving as an advisor. The author would also like to thank Scott A. Speakman and William Deane for their help with X-ray diffraction, and Jim Richardson and Evan Maxey for their help with neutron diffraction. The author would also like to thank Joeseph E. Spruiell, David C. Joy and Theodore C. Labotka for serving on the thesis committee.

Research sponsored by the Assistant Secretary for Energy Efficiency and Renewable Energy, Office of FreedomCAR and Vehicle Technologies, as part of the High Temperature Materials Laboratory User Program, Oak Ridge National Laboratory, managed by UT-Battelle, LLC, for the U.S. Department of Energy under contract number DE-AC05-00OR22725.

Research also supported by the Joint Institute for Neutron Sciences (JINS).

This work benefited from the funding by the Office of Science, US DOE to IPNS, ANL under contact #W-31-109-ENG-38 to the University of Chicago.

ABSTRACT

Hexacelsian, the hexagonal polymorph of $BaAl_2Si_2O_8$, experiences a phase transition near 300ºC with an accompanying large volume change, which can lead to cracking and thermal shock, limiting the potential applications of hexacelsian. It has previously been reported that certain additions, including MgO and TiO_2, can suppress the undesirable phase transition. Room-temperature neutron and high-temperature X-ray diffraction have been used to study the structure and thermal behavior of hexacelsian, both pure and substituted with varying amounts of MgO and TiO_2. The diffraction data of the pure sample was refined using the *P-3* space group. Attempting to refine the substituted sample with the same structure led to significant error due to peak intensity mismatch and the presence of extra peaks. The most likely explanation for the poor fit may be that the addition of Mg^{2+} and Ti^{4+} cations to hexacelsian significantly alters the structure in a way that has not been accounted for in the structural model thus far.

Additions up to 10mol% MgO and 6.67mol% TiO_2 did not suppress the α↔β transition near 300ºC in a solid-state synthesized sample. However, it has been previously claimed that additions of 5-25mol% MgO, 6-14mol% TiO_2, 0-10mol% ZnO, and 0-8mol% ZrO_2 would suppress the α↔β transition, when using melt-glass crystallization synthesis. Also, thermal expansion coefficients for solid-state synthesized samples were calculated and found to be lower than those previously reported for zeolite-derived synthesis. It may be concluded that the method of synthesizing pure and substituted hexacelsian affects the thermal properties and phase relationships.

TABLE OF CONTENTS

LIST OF TABLES

LIST OF FIGURES

LIST OF SYMBOLS AND ABBREVIATIONS

º	degree
Å	Angstrom
APB	anti-phase domain boundary
BAS	$BaAl_2Si_2O_8$
b_c	bound coherent scattering length
β_{SD}	statistically disorder β-hexacelsian
ºC	degrees Celsius
cm^{-1}	inverse centimeter
CMC	ceramic matrix composite
ΔL	change in length
ΔT	change in temperature
ΔV	change in volume
DSC	differential scanning calorimetry
DUC	Diffraction User Center
EPS	Earth and Planetary Sciences
EXPGUI	Exp Graphical User Interface
FAU	faujasite (Type X zeolite)
fm	femtometer
g	gram
GPPD	General Purpose Powder Diffractometer
GSAS	General Structural Analysis System
h	hour
HTML	High Temperature Materials Laboratory
IPNS	Intense Pulsed Neutron Source
IR	infrared
K	Kelvin

kcal	kilo-calorie
kJ	kilo-Joule
L_o	initial length
LTA	Linde type A zeolite
MAS NMR	magic angle spinning nuclear magnetic resonance
mg	milligram
mm	millimeter
MPa	MegaPascal
mol	mole
mol%	mole percent
NASA	National Aeronautics and Space Administration
ORNL	Oak Ridge National Laboratory
PDFC	Phase Diagrams for Ceramists
ppm	parts per million
RUM	rigid unit mode
SAED	selected area electron diffraction
sol-gel	solution-gelation
T	aluminum or silicon
U_{iso}	isotropic thermal parameter
U_{ij}	anisotropic thermal parameter
U.S.	United States
UTK	University of Tennessee, Knoxville
V_o	initial volume
Z	atomic number

1. INTRODUCTION

1.1 $BaO\text{-}Al_2O_3\text{-}SiO_2$ System

In the $BaO\text{-}Al_2O_3\text{-}SiO_2$ system, only one stable ternary compound exists ($BaAl_2Si_2O_8$ or BAS), as seen in Figure 1.1. Originally, BAS was known to exist in two different polymorphs, celsian and paracelsian. In 1931, Dittler and Lasch [1], investigating the synthesis of various feldspars, discovered a heretofore unknown polymorph of barium-aluminosilicate (BAS) with a hexagonal structure. Originally known as α-celsian, the newfound polymorph was later renamed hexacelsian [2].

Due to metastable behavior in the system, the true phase equilibrium relationships were unclear for several decades, until 1968. In that year, Lin and Foster [3], investigating previously proposed phase diagrams and conducting their own heating experiments, were able to construct a hypothetical phase diagram, Figure 1.2, with the correct phase equilibrium relationships.

Paracelsian, a naturally-occurring mineral found in Gwynedd, Wales [4], has a monoclinic structure and is metastable at all temperatures. Celsian, also a naturally occurring mineral with a monoclinic feldspar structure, is the stable phase of BAS up to 1590°C. Hexacelsian, found only as a synthetic product, is the stable phase from 1590 to 1760°C, at which temperature BAS melts. However, hexacelsian readily exists metastably at temperatures below 1590°C, and is more stable than paracelsian [3].

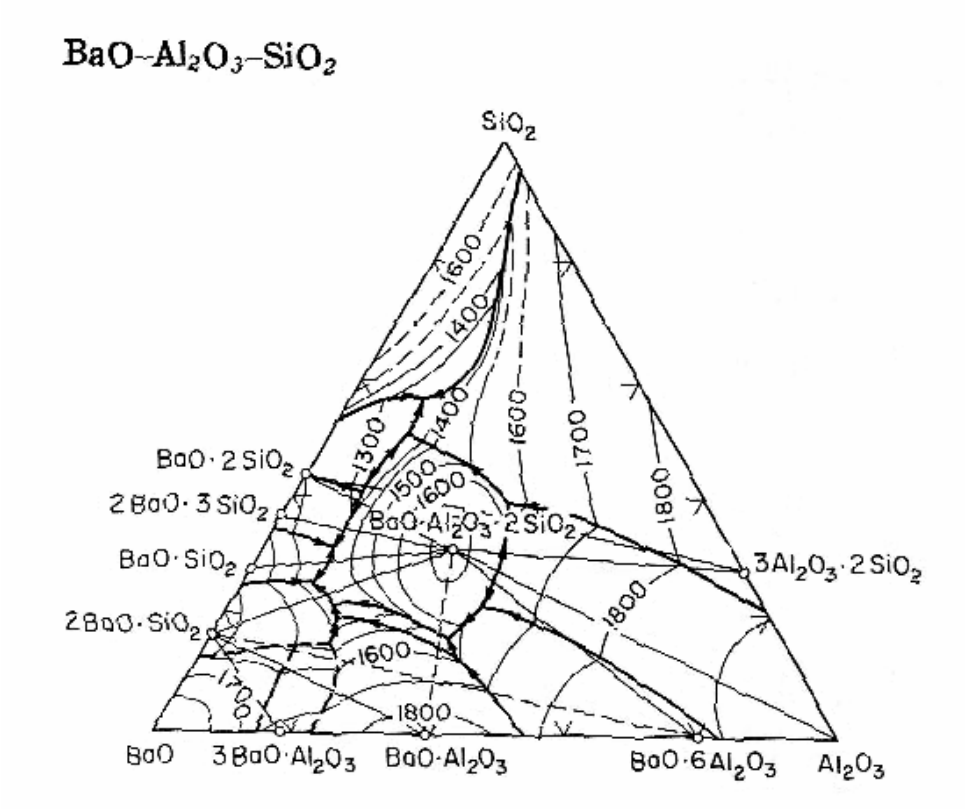

Figure 1.1 Phase diagram (PDFC #556) of the ternary BaO-Al_2O_3-SiO_2 system [5].

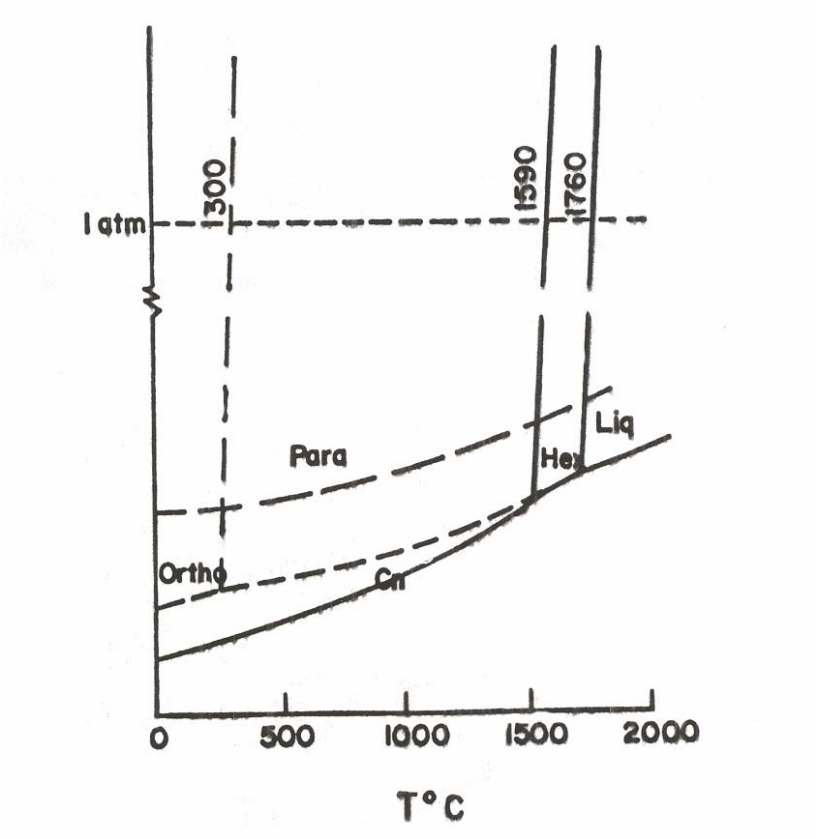

Figure 1.2 Hypothetical $BaAl_2Si_2O_8$ phase diagram of Lin and Foster [3]. Dotted lines indicate metastable relationships. Cn=celsian, Para=paracelsian, Hex=hexacelsian, Ortho=α-hexacelsian.

1.2 BAS Applications

BAS phases have several beneficial properties, including a high melting temperature, good oxidation resistance and, for celsian, a low thermal expansion coefficient [6-10]. Traditional applications of BAS phases include refractories [11] and electrical insulators [9]. More recently, much interest has focused on BAS, particularly celsian, as a matrix in ceramic matrix composites (CMCs) [7, 9, 12-15]. NASA has been interested in CMCs with a celsian matrix for high-temperature aerospace applications [10, 16].

1.2.1 Hexacelsian phase transition

Most of the research into BAS applications has focused on celsian, rather than hexacelsian. This is because hexacelsian undergoes a reversible phase transition around 300°C from α-hexacelsian (low temperature phase) to β-hexacelsian (high temperature phase). This phase transition is accompanied by a large volume change, which can lead to cracking, debonding and thermal shock. However, it is difficult to avoid forming hexacelsian. Even within the celsian equilibrium region of the phase diagram, hexacelsian will form first, and the hexacelsian → celsian transformation is slow. Much research has been devoted to preventing the formation of hexacelsian and speeding the hexacelsian → celsian transition [7, 16-20].

1.2.2 Stabilized hexacelsian

An opposite tack, instead of attempting to prevent hexacelsian, is to stabilize the thermal expansion of hexacelsian. In 1999, Beall et al. [21] received a patent for "Glass-ceramic containing a stabilized hexacelsian crystal structure". The authors used additions of MgO, TiO_2, ZnO and ZrO_2 to BAS in order to produce hexacelsian that did not experience a thermal expansion discontinuity. The authors envisioned the use of stabilized hexacelsian as a substrate for magnetic memory devices. Hexacelsian is well-

suited for this application due to good mechanical properties (fracture toughness, hardness and Young's modulus), capability of taking a fine polish with the use of conventional abrasives and being alkali-free (alkalis degrade magnetic coatings).

Rawn et al. [22] investigated hexacelsian both with and without MgO and TiO_2 additions with neutron diffraction at room temperature and 500°C. The addition of 15mol% MgO and 10mol% TiO_2 to BAS was found to suppress the α↔β phase transition. The addition of only MgO or only TiO_2 did not suppress the inversion; the presence of both was required. However, the information that could be drawn from the results was limited, due to the existence of a secondary phase, $MgTi_2O_5$.

1.3 Thesis Goals

This thesis aims to expand the line of research of hexacelsian stabilization by cation substitution. Hexacelsian samples, both pure and with varying amounts of MgO and TiO_2 additions have been synthesized using a solid-state method. High-temperature X-ray diffraction has been used to investigate the thermal expansion behavior and thermal stabilization of the hexacelsian samples. Neutron diffraction has been used to investigate the crystal structure and atom positions and occupancies, particularly those of the substitutional cations. The current research aims to investigate the mechanism by which the addition of MgO and TiO_2 affects the α↔β transition, and how the Mg^{2+} and Ti^{4+} ions fit within the hexacelsian structure.

2. BACKGROUND

2.1 Structural Determination by Diffraction

The structure of hexacelsian has been the source of much debate in the literature. The first structural investigation of hexacelsian was undertaken by Ito in 1950, though he referred to it as α-celsian [23]. Using X-ray diffraction, he determined the space group to be hexagonal *P6/mmm*, as seen in Figure 2.1, with one formula unit per unit cell. Ito refined lattice parameters of a = 5.25(3) Å and c = 7.84(1) Å. The structure consists of double layers of aluminum- or silicon-centered corner-sharing oxygen tetrahedra in a hexagonal arrangement. In between these double layers are single layers of barium ions. The barium is in twelve-fold coordination with the oxygen. The structure is referred to as a diphyllosilicate, indicating double sheets of aluminum and silicon tetrahedra [12].

The *P6/mmm* structure, though a decent beginning structure, has several problems. Firstly, twelve-fold coordination is unlikely unless the ions have the same radius, and barium and oxygen radii, though close, are still sufficiently different to cause problems. Also unfavorable are the linear T-O-T bonds (T = Al or Si) along the *c*-axis. Finally, *P6/mmm* has no means of distinguishing the aluminum and silicon ions, which are therefore randomly distributed between two equivalent crystallographic sites [24].

In 1951, Yoshiki and Matsumoto [2] reported X-ray diffraction and other results of hexacelsian produced by an electrofusion method. The X-ray diffraction results confirmed the existence of hexagonal symmetry. The dilatometric results indicated a large, reversible expansion on heating around 300°C. Specific heat measurements showed a discontinuity at the same temperature. From these results, Yoshiki and Matsumoto deduced the existence of a polymorphic phase transformation. In order to avoid confusion, the authors proposed the term “hexacelsian” for the hexagonal

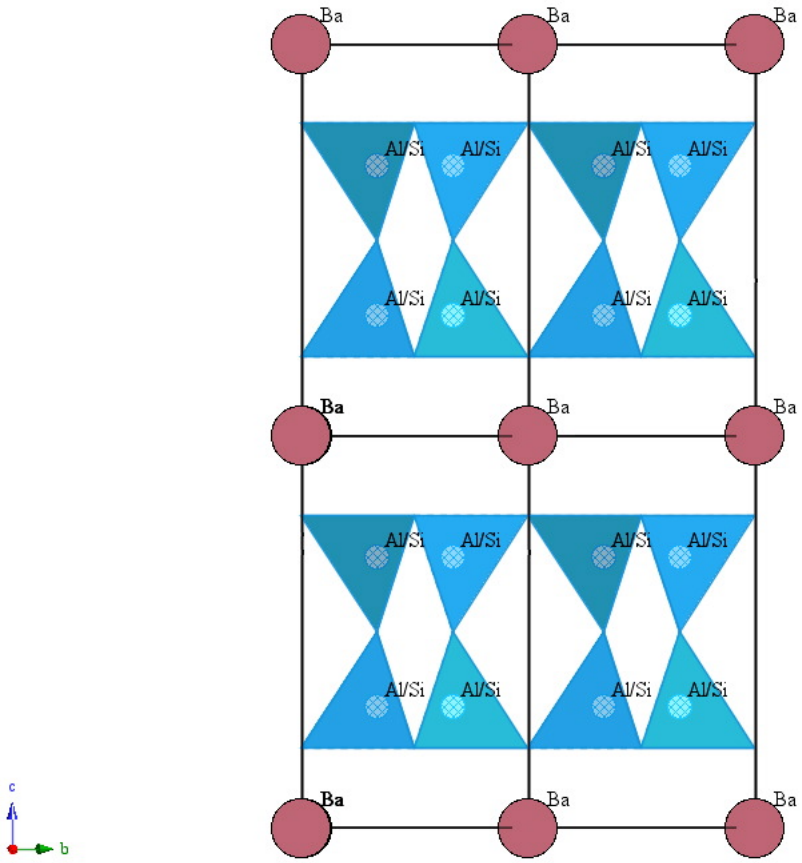

(a)

Figure 2.1 *P6/mmm* structure of hexacelsian from Ito [23]. The solid red spheres represent barium ions, the aluminum- and silicon-centered tetrahedra are blue. The crystal contains two unit cells in each direction, i.e. along the *a-, b-* and *c*-axes. Part (a) is viewed along the *a*-axis. Part (b) is viewed along the *c*-axis.

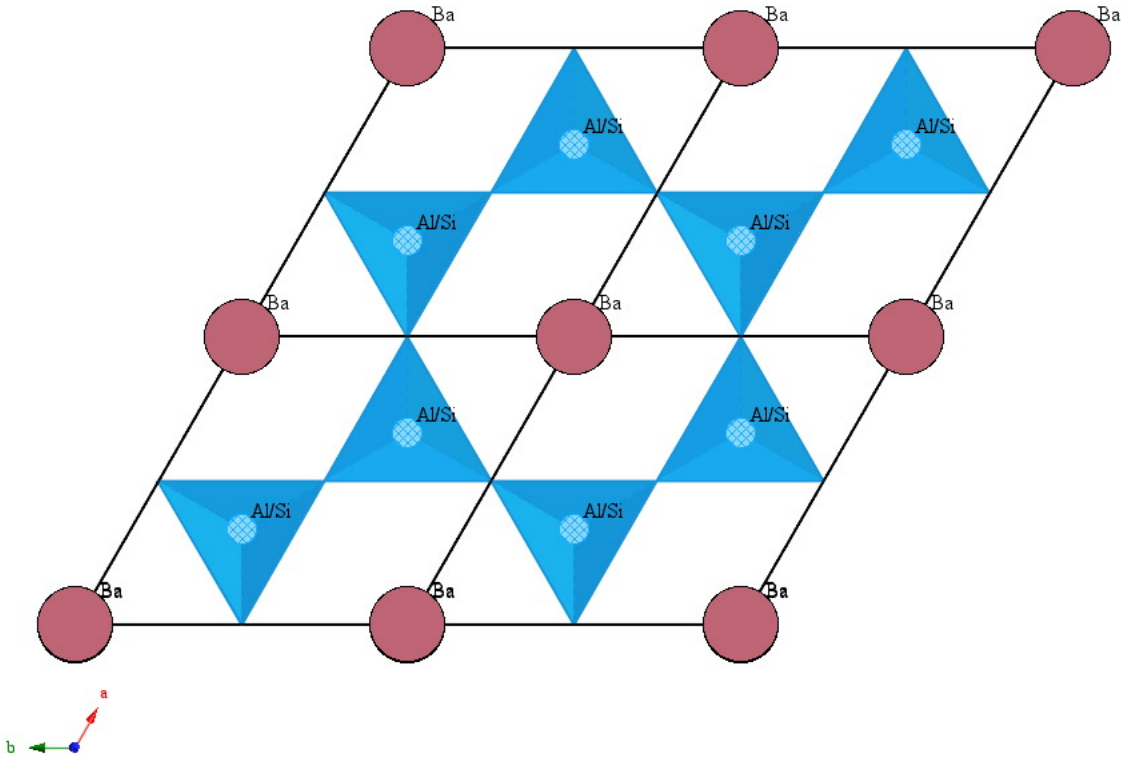

(b)

Figure 2.1 Continued.

polymorph of BAS, and α- and β-hexacelsian for the low- and high-temperature forms, respectively.

In 1953, Takéuchi, using X-ray diffraction, found that the β phase had true hexagonal symmetry [25]. He concluded that the α phase was body-centered orthorhombic, triply twinned so as to mimic a hexagonal structure. The orthorhombic structure has four formula units per unit cell, and the lattice parameters are related to the hexagonal cell by: $a_{ortho} = a_{hex}$, $b_{ortho} = a_{hex} * \sqrt{3}$, $c_{ortho} = 2c_{hex}$. The hexagonal layers are distorted into trigonal symmetry, by rotation of the tetrahedra along their axes parallel to the *c*-axis, resulting in a coordination number of six oxygen ions around each barium.

In 1977, Müller used hot stage transmission electron microscopy to study the α and β phases of hexacelsian [26]. He found two polymorphs at room temperature, $P6_3/mcm$ and *Immm*. The *Immm* phase corresponds to the pseudo-hexagonal body-centered orthorhombic phase identified by Takéuchi [25]. The $P6_3/mcm$ phase is hexagonal with a c-axis double that of the ideal *P6/mmm*. Müller concluded that the hexagonal ($P6_3/mcm$) phase was the low temperature α-phase and that the orthorhombic (*Immm*) phase was the high temperature β-phase. The existence of both at room temperature was concluded to be due to changes in local composition lowering the transformation temperature to below room temperature. $P6_3/mcm$ and *Immm* are both subgroups of *P6/mmm* and can therefore be derived from *P6/mmm* by losing some part of the symmetry. The observed anti-phase domain boundaries (APBs) in $P6_3/mcm$ and the observed APBs and twins in *Immm* are consistent with the loss of symmetry.

Müller hypothesized the existence of a second polymorphic transition in hexacelsian, from orthorhombic *Immm* (β) to hexagonal *P6/mmm* (γ) above 600°C. In 2002, Xu et al. found evidence to support Müller's hypothesis using hot-stage transmission electron microscopy [27]. Selected area electron diffraction (SAED) patterns were matched to calculated patterns for the expected structures. The γ-phase was further evidenced by the disappearance of twins and anti-phase domain boundaries found

in the β-phase. The authors determined that the β↔γ transition occurs around 700°C. The β↔γ transition was also investigated using differential scanning calorimetry (DSC) and dilatometry, and found to involve a small enthalpy of transformation and a small change in thermal expansion coefficient. The authors suggested that the small imprint of the transition accounted for it not previously being reported.

In the late 1990's, Kremenović et al., conducted X-ray studies on zeolite-derived hexacelsian [12, 28]. The authors refined both the α and β phases with the trigonal space group *P-3* (Figure 2.2), where the *a*- and *c*-axes correspond to those for the average *P6/mmm* structure. The hexagonal arrangement of aluminum- and silicon-centered tetrahedra is distorted into trigonal symmetry. The space group *P-3* has an advantage over the *P6/mmm* and derived space groups in that it distinguishes between the silicon and aluminum positions. The *P-3* structure still has problems, however, including the existence of linear T-O-T bonds. The β-phase was determined to be Al/Si disordered. The α-phase was determined to be Al/Si ordered, in accordance with the Loewenstein avoidance principle. This principle states that aluminum-centered tetrahedra preferentially bond to silicon-centered tetrahedra over other aluminum-centered tetrahedra, and vice versa. Such a preference would result in an alternating Al/Si order.

In 2000, Tabira et al. published the results of an electron diffraction study of phase transitions in hexacelsian [29]. At room temperature, the space group was determined to be body-centered orthorhombic *Immm*. The authors specifically looked for evidence of the space groups $P6_3/mcm$ and *P-3*, as had been previously proposed by Müller [26] and Kremenović et. al. [12, 28], respectively. No evidence was found for these space groups in pure hexacelsian at room temperature. However, in a lightly cesium-doped sample of hexacelsian, the authors found both *Immm* and $P6_3/mcm$ present at room temperature.

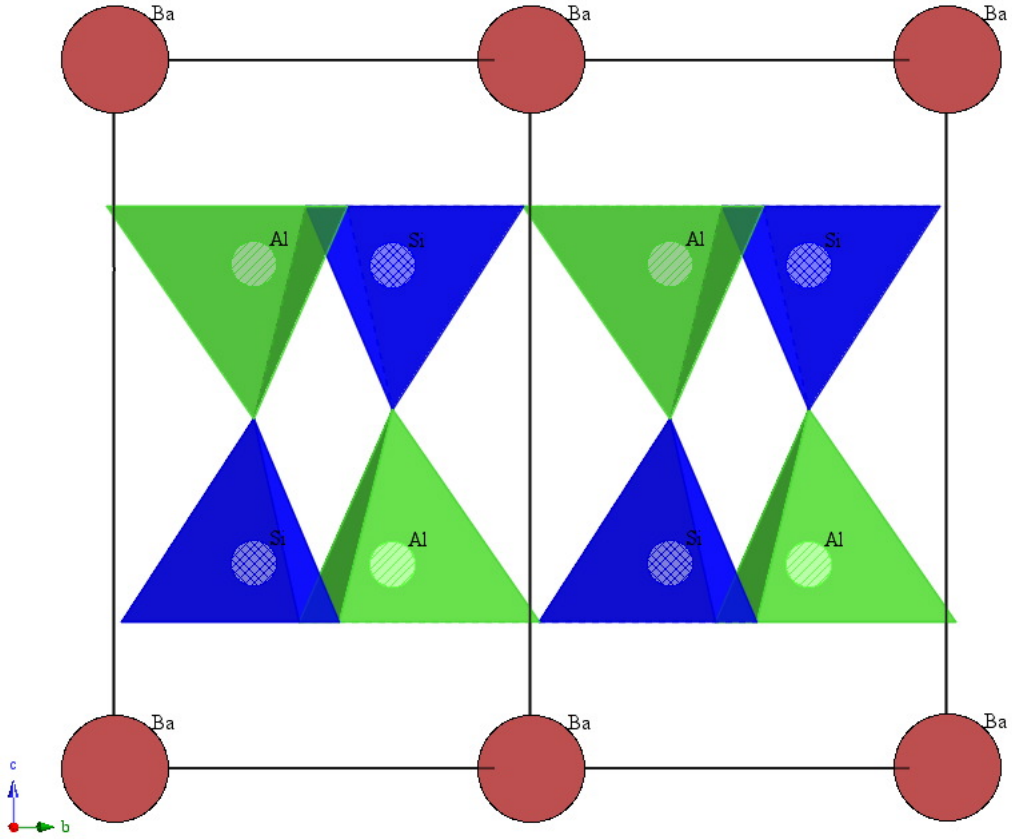

(a)

Figure 2.2 *P-3* structure of hexacelsian from Kremenović et al. [12, 28]. The solid red spheres represent barium ions, the aluminum-centered tetrahedra are green, with striped cations, and the silicon-centered tetrahedra are blue with cross-hatched cations. The crystal contains two unit cells in the *a*- and *b*-directions, and one unit cell in the *c*-direction. Part (a) is viewed along the *a*-axis. Part (b) is viewed along the *c*-axis.

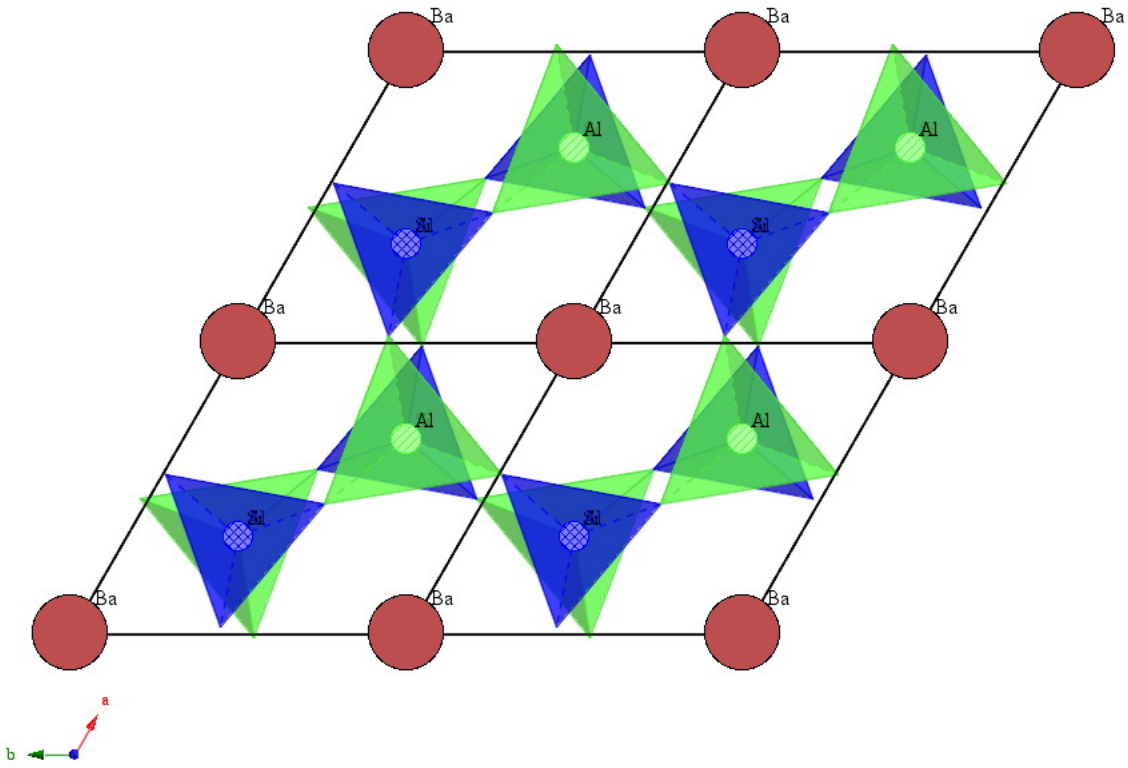

(b)

Figure 2.2 Continued.

2.2 Structural Determination by Spectroscopy

Because of the close relationship between the symmetry of the α and β phases, their X-ray patterns are similar. Therefore, it may be easier to distinguish the phases using spectroscopic techniques. In 2000, Colomban et al. combined IR (infrared) and Raman spectroscopy with X-ray diffraction in order to study the α↔β transition in sol-gel synthesized hexacelsian [30]. Both IR and Raman spectra show differences between the two phases. In the IR spectra, differences are seen in the relative intensities of the 205/225 cm^{-1} doublet and of the 362/400 cm^{-1} doublet. In α-hexacelsian, the 205 and 362 cm^{-1} bands are strong, while in β-hexacelsian, the 225 and 400 cm^{-1} bands are strong. In the Raman spectra, bands at 183 and 479 cm^{-1} are stronger in the α-phase, and the band at 59 cm^{-1} is stronger in the β-phase. Colomban et al. also noticed band broadening in the β-phase, confirming the order-disorder aspect of the α↔β transition, which had been previously reported [12, 28].

The Raman band at 810 cm^{-1} in the α-phase was absent in the IR spectrum. IR spectroscopy is subject to selection rules, such that only vibrational modes that result in a change in the dipole moment of the structure will be detected. When a symmetric structure is subjected to a symmetric vibrational mode, there is no change in the dipole moment, and that mode cannot be detected with IR spectroscopy. Raman spectroscopy works on a different principle with different selection rules, and therefore, a symmetric mode in a symmetric structure will be detected [31]. The IR/Raman exclusion of the 810 cm^{-1} band indicates that a center of symmetry exists in the α-phase. The IR/Raman exclusion in the α-phase was also reported by Kremenović et al. [32] in a later study. No such exclusion was seen in the β-phase, indicating the absence of a center of symmetry.

In 2003, Kremenović et al. published the results of a study of hexacelsian using ^{27}Al and ^{29}Si MAS NMR (Magic Angle Spinning Nuclear Magnetic Resonance) and Raman, IR and luminescence spectroscopies [32]. ^{27}Al and ^{29}Si MAS NMR spectra were

collected in order to investigate the Al/Si ordering of the β-phase. Four distinct silicon peaks indicated the existence of four distinct silicon environments, confirming the disorder in the β-phase. From the ^{29}Si MAS NMR data, the mean T-O-T (T = Si or Al) bond angles for the four distinct silicon environments were determined to be 139.1°, 140.5°, 142.6°, and 146.4°. These values are reasonably close to that for the *P6₃/mcm* space group, 146°. Therefore this structure does not have the unfavorable linear T-O-T bonds, which are present in the *P6/mmm* and *P-3* structures.

The authors further investigated hexacelsian using X-ray diffraction. From the X-ray data of Eu^{3+}-doped hexacelsian, they determined the space group of the ordered α-phase to be *P-3*, in agreement with Kremenović's earlier work [12, 28]. However, the space group of the disordered β-phase was determined to be *P6₃/mcm*, contrary to Kremenović's earlier work. This is the same space group that Müller found in 1977 [26], though he assigned it to the α-phase. Attempts to locate the europium ion within the unit cell resulted in insignificant refined site occupancies, indicating a negligible effect on the structure.

2.3 Polymorphic α↔β Transition in Hexacelsian

In 1978, Bahat [18] investigated various polymorphic transitions in hexacelsian and its strontium and calcium analogs, along with quartz. He found that the α↔β transition in hexacelsian is both displacive, i.e. involving a minor alteration of the structure, and homogeneous, i.e. occurring simultaneously throughout the bulk. Bahat also investigated the order of the transition. Phase transitions are 1st order if the extensive properties (the first derivates of Gibbs free energy) change discontinuously at the transition; 2nd or higher order transitions do not show a discontinuity in the extensive properties. In hexacelsian, the volume exhibits a discontinuity at the α↔β transition. Bahat determined that the transition proceeds as a higher order transition, due to

simultaneous bond stretching, before abruptly ending as a 1st order transition, due to the sudden release of accumulated strain.

Bahat also investigated the effect of impurities on the α↔β transition. He found that the 1st order character of the transition diminished when impurities were added in solid solution. Bahat postulated that this indicated a change in the character and mechanism to a heterogeneous, higher order transition, due to the absence of strain buildup. Bahat also pointed to the possibility that the α↔β transition could be affected by the degree of order/disorder in the structure, which could be in turn affected by impurities and/or cooling history.

Kremenović et al. also studied the α↔β phase transition in hexacelsian [12, 28]. They found a discontinuity of the thermal expansion, indicating that the α↔β transition was ferroelastic, i.e. involving a deformation of the unit cell. The absence of a change in symmetry (both phases were refined with *P-3*) was taken to indicate that the transition was non-convergent. The authors hypothesized that the α↔β transition was affected by two processes: one, distortion of the double six-member tetrahedral rings and of the BaO_6 octahedra, and two, ordering of the aluminum and silicon cations.

2.4 Dynamic Vibrational Modes in Hexacelsian

The effects of dynamic modes of vibration on the α↔β↔γ transitions have also been studied. Colomban et al. [30] assigned Raman spectrum bands of the ordered α-phase to specific vibrational modes. For this purpose, the hexacelsian structure was conceptualized as isolated SiO_4 tetrahedra with aluminum ions sitting in tetrahedral sites between the SiO_4 tetrahedra. A strong band at 103 cm^{-1} was assigned to a translation vibrational mode of the tetrahedra layer. A strong band at about 404 cm^{-1} was assigned to a bending mode of the isolated tetrahedra. A medium band at 810 cm^{-1}, which does

not appear in the IR spectrum, was assigned to a symmetric stretching mode of the tetrahedra. A group of medium-to-weak bands in the range of 900-1250 cm^{-1} was assigned to asymmetric stretching modes of the tetrahedra. In a later study [32], the 103 cm^{-1} band, which had been assigned to translation lattice vibrations of the tetrahedra layer in the previous paper by Colomban et. al. [30], was reassigned to translation vibrations of the Ba^{2+} layer.

In the previously discussed electron diffraction study by Tabira et al. [29], the authors noticed strong diffuse scattering streaks in the higher temperature β-phase as well as in the cesium- and rubidium-doped samples. These streaks disappeared in the lower temperature α-phase. The authors hypothesized that the diffuse streaking was due to vibrational modes of the β-hexacelsian structure. To be specific, they proposed columns of silicon- or aluminum-centered tetrahedra in the <110> direction, in which the tetrahedra rotate along their *c*-axes, independent of neighboring columns. The two layers of tetrahedra within each double layer rotate in the same direction. Withers et al. investigated the vibrational modes of hexacelsian further in a second paper [24] discuss below in section 2.4.1.

2.4.1 Computer modeling of vibrational modes

The vibrational modes of hexacelsian were modeled using a lattice dynamics computer program called CRUSH. The two-dimensional nature of the average *P6/mmm* structure allows essentially zero frequency vibrational modes, which result in structural flexibility. The Si-O and Al-O bonds are significantly stronger than the Ba-O bonds. So the energy required to distort the tetrahedra is much greater than that to rotate the tetrahedra. Therefore, the authors modeled the structural vibrations using rigid unit modes (RUMs). In a RUM, the coordination polyhedra, in this case tetrahedra, are assumed to be non-distortable, and all structural vibrations are due to changes in orientation between the polyhedra.

Using the CRUSH program, three different zero-frequency RUMs, labeled types I, II and III, were discovered for the average *P6/mmm* structure. Type I RUMs correspond to the vibrational mode proposed in the previous paper [29], i.e. rotations of tetrahedra about their *c*-axes in independent <110> columns. The diffuse scattering streaks observed in the electron diffraction pattern of the β-phase confirm that type I RUMs are the dominant vibrational mode of the β-phase. Type II RUMs correspond to the rotation of the tetrahedra along an axis that runs through the basal planes of the tetrahedra. The existence of type II RUMs allows the presence of non-linear T-O-T (T = Si or Al) bonds, the absence of which was a problem with most of the earlier proposed structures. Type III RUMs are similar to type I RUMs, except that the two layers of tetrahedra within each double layer rotate in opposite directions, not in the same direction.

The authors proposed that in the highest temperature γ-phase, all RUMs are active, combining to form the average *P6/mmm* structure. Though on average there appear to be linear T-O-T (T = Si or Al) bonds, due to the combination of RUMs, the T-O-T bonds are not linear at any point in time. Upon cooling, at specific temperatures, certain RUMs will become inactive, in effect 'freezing' or 'condensing' out, resulting in a phase change. The first RUMs to freeze out are type II RUMs, resulting in a phase change from *P6/mmm* to orthorhombic *Ibmm* ($a = a_o + b_o$, $b = -a_o + b_o$, $c = 2c_o$). This corresponds to the γ↔β phase transition. At approximately 300°C, the type I RUMs freeze out, which combined with the previously frozen out type II RUMs, results in a phase change from *Ibmm* to orthorhombic *Ib2m*. This corresponds to the β↔α phase transition. If ordering of the aluminum and silicon in the α-phase is taken into account, then the symmetry reduces to *Ib11*. The sequence proposed in this paper relieves certain problems with prior proposals, i.e. linear T-O-T bonds. However, it does not adequately explain the clearly documented order/disorder transition.

2.5 Hexacelsian → Celsian Transformation

In addition to studies on the polymorphic transitions within hexacelsian, several studies have been produced concerning the transformation from hexacelsian to celsian. In 1970, Bahat [17] found that the hexacelsian → celsian transformation was sluggish, particularly in large particles. The reaction rate was fastest in powder at 1250°C. Grain size was found to be the primary variable affecting the rate of the transition. Bahat determined that the sluggish transformation rate was due to a lack of nucleation, and that the grain size effect was due to an increase in heterogeneous nucleation sites at lattice defects and interfaces when decreasing the grain size. Bahat also found that the hexacelsian → celsian activation energy was 20.1 kcal/mol (84.2 kJ/mol), lower than the approximately 60 kcal/mol (250 kJ/mol) required for breaking silicon-oxygen and aluminum-oxygen bonds.

These results led Bahat to conclude that the hexacelsian → celsian transformation did not involve diffusion or breaking silicon-oxygen or aluminum-oxygen bonds, and instead was due to small changes in the orientation and arrangement of the silicon- and aluminum-centered tetrahedra. However, in a further study published in 1978 [18], Bahat amended his hypothesis to include the presence of diffusion of barium ions in the hexacelsian → celsian transformation. He determined from the difference in densities of hexacelsian and celsian that diffusion must occur. This is further evidenced by the fact that the transition is quenchable, i.e. can be suppressed with a sufficiently fast cooling rate, indicating that a time-dependant process, such as diffusion, is instrumental in the transition. In addition, Bahat noted that the hexacelsian → celsian transition is reconstructive because of the absence of any relationship between their crystal structures.

In 2001, Kobayashi investigated the kinetics of the hexacelsian → celsian transformation [7]. Hexacelsian powders of varying particle size were heated at temperatures from 300 to 400°C for times up to approximately 80 hours, and the extent of the transformation was measured using X-ray diffraction. A modified first order

equation was used to calculate nucleation and growth rate constants and activation energies from the data. Kobayashi postulated that the sluggishness of the hexacelsian → celsian transformation was due to a low crystal growth rate. The calculated nucleation and growth activation energies were 407 and 228 kJ/mol, respectively. These values are significantly greater than the activation energy previously calculated by Bahat (84.2 kJ/mol) [17].

2.6 Hexacelsian Synthesis

Several different methods have been utilized to synthesize hexacelsian. In addition to standard solid-state synthesis [1, 6, 9, 33-35], hexacelsian has also been crystallized from glasses of the desired composition. These glasses have been formed from a melt [16, 20, 36], through a sol-gel process [30, 37-40], or by zeolite transformation [8, 12, 28, 41-45]. More rarely, hexacelsian has been synthesized by oxidation [46, 47], electrofusion [2], and dehydration of cymrite ($BaAl_2Si_2O_8 \cdot H_2O$) [48].

2.6.1 Solid-state synthesis

In its first recorded appearance [1], hexacelsian was synthesized by a solid-state process. In the solid-state synthesis of hexacelsian, BaO, or more commonly $BaCO_3$, is mixed with SiO_2 and Al_2O_3, or with kaolin, $Al_2Si_2O_5(OH)_4$. The mixture is heated at elevated temperatures to cause the constituents to react and form hexacelsian. Lee and Aswath [9, 33] found that hexacelsian could form via two different reaction paths. In the first, $BaCO_3$ reacts with Al_2O_3 to form $BaAl_2O_4$, which then reacts with SiO_2 to form hexacelsian. In the second, $BaCO_3$ reacts with SiO_2 to form $BaSi_2O_5$, which then reacts with Al_2O_3 to form hexacelsian. The second reaction proceeds faster than the first. Therefore Lee and Aswath determined that hexacelsian could be yielded more quickly by

prefiring $BaCO_3$ and SiO_2 before firing with Al_2O_3 to prevent the formation of $BaAl_2O_4$. Specifically, pure hexacelsian was formed by firing $BaCO_3$ and SiO_2 in a 1:2 molar ratio at 1150°C for 4 hours, and then firing the resulting powder in a 1:1 molar ratio with Al_2O_3 at 1200°C for 6 hours.

2.6.2 Melt glass crystallization

By grinding kaolin and $BaCO_3$ and heating the mixture up to 800°C, Okada et al. [34] formed an amorphous BAS material. Despite band broadening in the amorphous sample, the ^{27}Al and ^{29}Si MAS NMR spectra of the glass and a hexacelsian sample were very similar, leading the authors to conclude that the short-range order in the glass is similar to that in hexacelsian. If correct, the barrier to crystallization of hexacelsian from the glass could be expected to be lower than that for celsian, even at temperatures within the celsian equilibrium region. Indeed, Drummond et al. [16], studying the crystallization of a BAS glass quenched from a melt, found that the first phase to crystallize, at a range of temperatures up to 1290°C, was hexacelsian.

In a later, more in-depth study, Hyatt and Bansal [20] found that for a heating time of one hour, a fully hexacelsian sample was obtained at 1000°C (in powder) and celsian began to form at 1100°C. For a heating time of ten hours, the sample was fully hexacelsian at 950°C, and celsian began to form at 1050°C. Hexacelsian was found to be surface nucleated, and celsian was found to form by transformation from hexacelsian, not by directly crystallizing from the glass. Hyatt and Bansal suggested that hexacelsian has a lower nucleation kinetic barrier due to its simpler, higher-symmetry structure.

2.6.3 Sol-gel synthesis

BAS glass powders have also been generated, without the need of the high temperatures required for melting, using the sol-gel synthesis method. All of the reported sol-gel routes used tetraethyl orthosilicate ($Si(C_2H_5O)_4$), or TEOS), as the source of

silicon, and Al-*sec*-butoxide ($Al(C_4H_9O)_3$) as the source of aluminum. As a source of barium, the different routes used barium metal [37, 39, 40], barium acetate ($Ba(C_2H_3O_2)_2$) [40, 49], barium hydrate ($BaH_2O_2 \cdot 8H_2O$) [30], or barium isopropoxide ($Ba(C_3H_7O)_2$) [38]. The resulting glass powders were crystallized to hexacelsian at temperatures ranging from 950 to 1200°C.

All studies found that hexacelsian crystallized from the glass powders before celsian. Chen et al. [37] attributed this to the lower Al/Si order in β-hexacelsian. Winter [49] attributed the preference for hexacelsian crystallization to the larger barium site in hexacelsian than in celsian, improving the diffusion kinetics. Several researchers found that the certain additions, such as Li_2O [38] and TiO_2 [40], favored the formation of celsian, a finding that was also reported in melt glass crystallization [16]. Lee et al. [39] compared the crystallization behavior of BAS glasses obtained via melt and sol-gel methods. Melt glass was found to crystallize on the surface, while sol-gel glass crystallized in the bulk. The authors speculated that the difference in nucleation site was due to differences in the local structure of the melt and sol-gel glasses.

2.6.4 Zeolite derivation

Zeolites are tectosilicates, as is celsian. Tectosilicates, which have three-dimensional framework structures of corner-sharing aluminum- and silicon-centered tetrahedra, are divided into three groups based upon the size of their polyhedral cavities: pyknolites, clathrasils and zeolites. Pyknolites, which include celsian, have small polyhedral cavities filled with cations. Clathrasils have cavities sufficiently large to hold cations and molecules, but openings too small to allow them to escape. Zeolites have large cavities connected by large openings and channels, which allow the flow of cations and molecules into and out of the structure. The two zeolites of interest in the synthesis of BAS are zeolites A (or Linde type A, abbreviated LTA) and X (or faujasite, abbreviated FAU). Zeolites A and X consist of β-cages of truncated octahedra arranged in simple cubic and diamond-type lattices, respectively [50].

Because of the open structures of zeolites, their cations may easily be exchanged for other species. In 1991, Corbin et al. [51] used this principle to exchange the sodium in zeolites A and X for barium. Once the sodium was exchanged for barium, heat was applied, causing the zeolite to collapse into an amorphous structure, which was then crystallized into BAS. In 1994, Hoghooghi et al. [8] used a similar technique to form hexacelsian. Barium was exchanged into zeolite X, the sample was vitrified at temperatures up to 900°C, and then the glass was crystallized to hexacelsian at temperatures up to 1200°C for three to four hours.

McKittrick et al. [41] further investigated the synthesis of hexacelsian via zeolite X cation-exchange and compared the zeolite glasses to glasses formed by other methods. The Ba-exchanged zeolite vitrified around 610-630°C, and the zeolite-glass crystallized into hexacelsian around 1000-1100°C. The authors found that the zeolite-glass was less dense than BAS glass derived from other methods, most likely due to the open zeolitic structure from which it was derived.

Djordjevic et al. [43] investigated the structure of BAS glass derived from zeolite A. The zeolite-glass was determined to have a layered structure with barium ions between the layers, and a barium coordination of twelve (as compared to six in the zeolite). This is in accordance with Okada et al. [34] who found that the BAS glass had a local structure similar to hexacelsian. In addition, Djordjevic et al. found that the aluminum/silicon order in the zeolite was retained in the glass.

2.7 Synthesis of Statistically Disordered β-Phase

Kremenović et al. [12, 28] compared hexacelsian derived from zeolite A to that derived from zeolite X. Zeolite A resulted in a stoichiometric hexacelsian, while zeolite

X resulted in a non-stoichiometric hexacelsian. Thermal expansion investigations showed that while the zeolite A hexacelsian underwent the α↔β phase transition near 300°C, the zeolite X hexacelsian did not [28]. Zeolite A hexacelsian was found to be aluminum/silicon ordered at room temperature, as expected according to the results of Djordjevic et al., who found that the aluminum/silicon order in zeolite A was retained in the glass. On the other hand, zeolite X hexacelsian was found to be aluminum/silicon disordered even at room temperature. In addition, Kremenović et al. [32] found that even stoichiometric zeolite A hexacelsian could be synthesized into the β-phase at room temperature if quenched from 990°C.

This disordered β-hexacelsian found at room temperature is referred to as β_{SD} (Statistically Disordered). Such a phase could be very beneficial for many applications, as it would not undergo the α↔β phase transition, with accompanying volume change, which limits the use of hexacelsian. In addition to zeolite X derivation, several other paths have been found to produce β_{SD}, namely compositional changes and sol-gel synthesis.

It is possible to prepare non-stoichiometric hexacelsian in a range of compositions with the forms $Ba_{1-x}Al_{2-2x}Si_{2+4x}O_8$ and $Ba_{1+x}Al_2Si_2O_{8-x}$ [30]. Müller found both *P6₃/mcm* and *Immm* at room temperature, and found that the α-phase was stoichiometric, while the β-phase was not [26]. He concluded that altering the stoichiometry from the ideal lowered the α↔β transition temperature below room temperature. Doping with metal cations has also been found to suppress the α↔β inversion. Beall et al. [21] found that the addition of MgO, TiO_2, ZnO, and ZrO_2 in varying quantities resulted in hexacelsian that did not undergo the α↔β phase transition near 300°C. The effect of MgO and TiO_2 additions was also studied using neutron diffraction by Rawn et al. [22], though the results were limited due to the presence of secondary phases in the samples.

Colomban et al. [30] investigated sol-gel synthesized hexacelsian using barium hydrate. It was found that sol-gel glass powders sintered at 1150°C for up to 24 hours crystallized into the β_{SD} phase, while samples sintered for 96 hours formed the α-phase. The authors hypothesized that the gelation step of the sol-gel synthesis method froze in Al/Si disorder resulting in the β_{SD} phase. The longer annealing times allowed the aluminum and silicon to order, resulting in the α-phase.

3. EXPERIMENTAL PROCEDURE

3.1 Sample Synthesis

3.1.1 Solid-state synthesis method

Both the pure and substituted hexacelsian samples were synthesized using a solid-state method. In this synthesis method, precursor oxide powders are mixed in a stoichiometric ratio to give the desired final composition. The powders are pressed into a pellet, and then fired in multiple steps of increasing temperature, until the desired phase is formed. This is generally achieved by heating to a temperature within the equilibrium region of the phase diagram for the desired phase, and then holding at that temperature for a sufficient time to reach equilibrium.

3.1.2 Sample compositions

The compositions of the samples discussed in this thesis are given in Table 3.1. (The compositions of all samples synthesized are in Table A.1 in the appendix.) Throughout this thesis, samples are identified with the target amount of additions. The precursor oxides powders were $BaCO_3$ (Fisher Scientific, 99.5%), Al_2O_3 (Alfa Aesar, 99.995%), SiO_2 (Alfa Aesar, 99.5%), MgO (Fisher Scientific, 97.0%) and TiO_2 (Fisher Scientific, 99.9%). The precursor powders were held in a drying oven at 120°C in order to drive off any residual water, which might affect the mass. The powders were massed using a Fisher Scientific balance (d = 0.1 mg). The mixed precursors were pressed uniaxially using a Carver hydraulic hand press with pressures around 700 MPa.

Table 3.1 Selected sample compositions in grams and mole percent.

Sample	$BaCO_3$		Al_2O_3		SiO_2		MgO		TiO_2	
	g	**mol %**	**g**	**mol %**	**g**	**mol %**	**g**	**mol %**	**g**	**mol %**
pure	1.0515	25.00	0.5433	25.00	0.6402	50.00	--	--	--	--
15-10 melt synthesis	2.6293	18.75	1.3585	18.75	1.6014	37.50	0.4297	15.00	0.5679	10.00
15-10 solid state synth.*	2.6293	23.26*	1.3294	22.77*	1.0612	46.53*	0.1031	4.466*	0.1361	2.974*
10-6.67	2.8166	20.83	1.4552	20.83	1.7153	41.67	0.2761	10.00	0.3652	6.671
7.5-5	1.4525	21.87	0.7506	21.88	0.8846	43.75	0.1017	7.498	0.1344	4.999
5-3	3.0001	23.00	1.5503	23.00	1.8269	46.00	0.1333	5.002	0.1586	3.003

* Amounts in mole percents are incorrect due to BaO, Al_2O_3 and SiO_2 loss before MgO and TiO_2 addition.

3.1.3 Heat treatment

The sample heat schedules are represented in Figure 3.1. (Full heat schedules are given in Tables A.2 and A.3 in the appendix.) In general, the samples were first calcined at 800-850°C, then heated in larger temperature increments up to approximately 1400°C, and then further heated in smaller temperature increments up to the hexacelsian equilibrium region (above 1590°C). The samples were generally heated for 24 hours per step. All heat treatment was conducted in an air atmosphere. Either a sacrificial pellet or platinum foil was used to isolate the samples from the alumina boats in which they where fired. The samples were generally furnace-cooled. Between heating steps, the samples were crushed using an agate mortar and pestle and milled using a Fritsch Pulverisette vibratory mill before being pressed and heated again.

Three furnaces were used: a box furnace with a maximum temperature of 1200°C (Micropyretics Heaters International Z12), a box furnace with a maximum temperature of 1700°C (CM Furnaces, Incorporated 1706FL), and a horizontal tube furnace also with a maximum temperature of 1700°C (CM Furnaces, Incorporated 1730HTF). Some error exists in the temperature measurements due to placement of the sample five to ten centimeters away from the thermocouple.

3.1.4 Alternate synthesis methods

Samples with 15mol% MgO and 10mol% TiO_2 were unable to be synthesized using the solid-state method, due to secondary phases causing melting at temperatures much lower than expected. Therefore, synthesis was attempted using two other methods: melt glass crystallization and a two-step solid-state method. In the first case, a sample previously heated up to 1460°C was melted at 1650°C in a platinum crucible and furnace cooled to room temperature. The sample was crushed, and the resulting powder was heated at 1000-1100°C in order to crystallize hexacelsian.

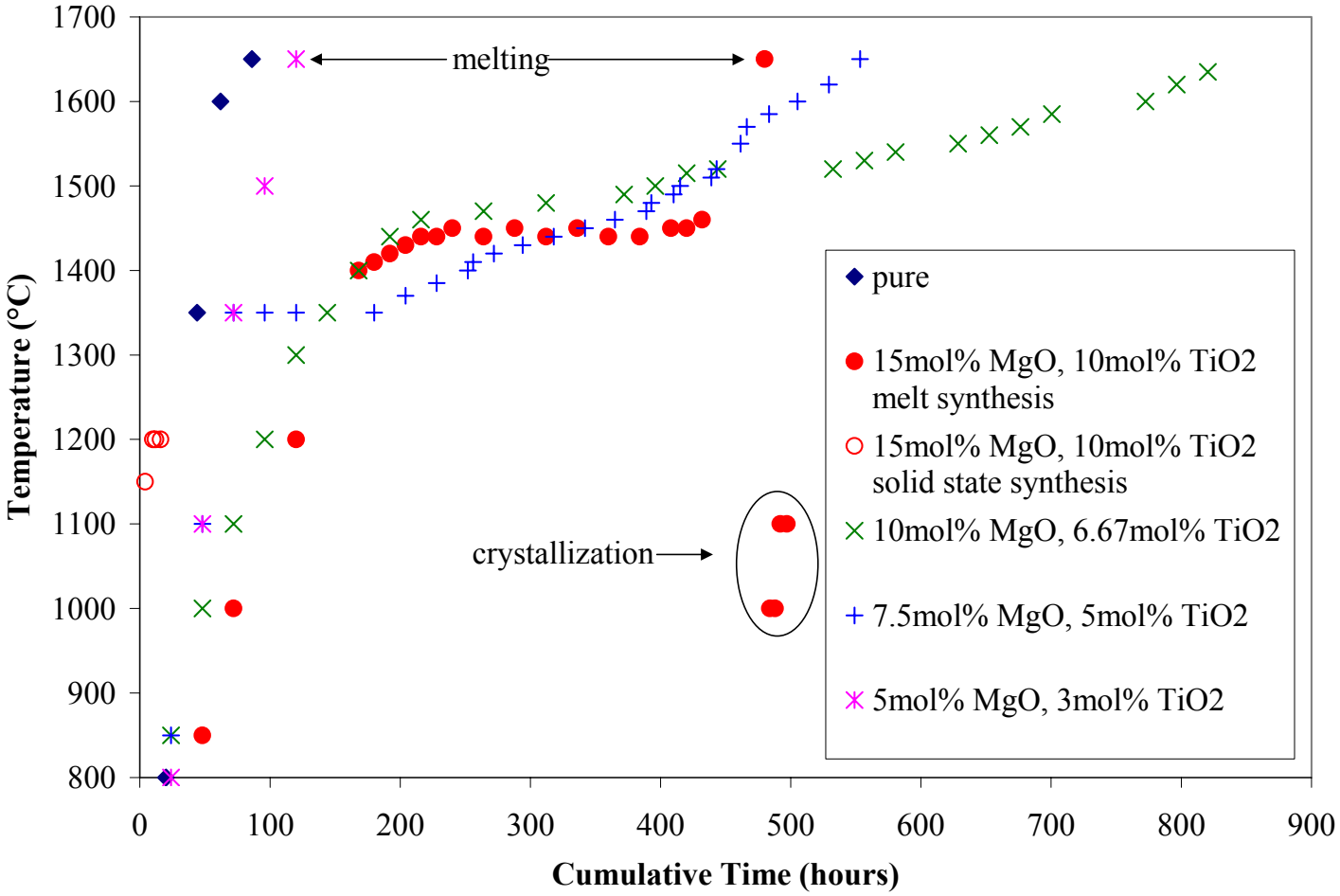

Figure 3.1 Heating schedules, as temperature versus total time of heat treatment. Therefore, the time difference between two data points represents the length fo time held at the temperature of the first data point.

The two-step solid-state method was outlined by Lee and Aswath [9, 33]. A 1:2 molar ratio of $BaCO_3$ to SiO_2 was heated at 1150°C for 4 hours. The resulting powder was mixed in a 1:1 molar ratio with Al_2O_3 and heated at 1200°C for 8 hours. Finally, additions of 15mol% MgO and 10mol% TiO2 were added, and the sample was heated at 1200°C for 4 hours. The firing times are shorter than those for standard solid-state synthesis. Unlike the previous method, the goal of multiple-step solid-state synthesis is to form a metastable phase, i.e. hexacelsian, and avoid the equilibrium phase, i.e. celsian.

3.1.5 Sol-gel synthesis

A pure sample was also synthesized using the sol-gel (solution-gelation) method. In this synthesis method, solutions of chemical agents, often organics, containing the desired species are mixed. The solutions react, while being stirred, to form a gel, in which the desired species are intimately mixed. The gel is dried to form a xerogel, which is then ground. Finally, the resulting amorphous powder is crystallized by heat treatment. The advantage of sol-gel synthesis is the formation of an amorphous material at temperatures far below those required for melting.

A sol-gel method to form hexacelsian outlined by Liu et al. [40] was used. Water (0.7675 g) and tetraethyl orthosilicate, or TEOS ($Si(C_2H_5O)_4$), (4.4322 g) were mixed in a 2:1 molar ratio. Ethanol and aluminum-*sec*-butoxide ($Al(C_4H_9O)_3$) (2.6289 g) were mixed in a 3:1 volume ratio. The two solutions were mixed together along with an aqueous solution of barium acetate ($BaC_4H_6O_4$) (2.7216 g) and stirred overnight at room temperature. The resulting gel/powder mixture was dried at 115-120°C for two to three days. The resulting powder was then fired in air at 600 and 800°C for 24 hours per step.

3.2 Diffraction Data Collection

3.2.1 Room-temperature X-ray diffraction

Room-temperature X-ray diffraction data were collected on two different diffractometers. A Siemens Kristalloflex θ-θ diffractometer (in the X-ray laboratory of the Earth and Planetary Sciences (EPS) department at the University of Tennessee, Knoxville (UTK)) was used for phase identification. The diffractometer used Cu K_α radiation with a monochromator; the samples were held in plastic deep well holders. Large amorphous bumps centered near 2θ=12º in the diffraction patterns taken with this instrument are artifacts due to the sample holders. A Scintag θ-2θ diffractometer (in the Diffraction User Center (DUC) in the High Temperature Materials Laboratory (HTML) at Oak Ridge National Laboratory (ORNL) in Oak Ridge, Tennessee) was also used for room-temperature X-ray diffraction. This diffractometer used Cu K_α radiation with nickel filters to absorb K_β radiation. Both deep-well and side-load sample holders were used.

3.2.2 High-temperature X-ray diffraction

It is desirable to use parallel beam optics when collecting high-temperature X-ray diffraction data. The parallel beam geometry is insensitive to peak position inaccuracy due to sample surface displacement. This effect can be considerable due to thermal expansion of the sample as it is heated. It is also desirable to use a linear position sensitive detector. When many patterns are being collected, the ability to detect a range of 2θ angles at once greatly speeds data collection. However, position sensitive detectors are not designed to be used with parallel beam optics. It was shown in a previous research project by the author, Scott A. Speakman and Claudia J. Rawn [52] that use of a position sensitive detector negates the insensitivity of a parallel beam to sample surface displacement. Therefore, it was decided to use Bragg-Brentano parafocusing beam optics

with a position sensitive detector for the current research. The sample surface displacement was accounted for in the refinement of the data.

High-temperature X-ray diffraction data were collected on a PANalytical X'Pert Pro θ-θ diffractometer, also a DUC instrument. This diffractometer used Cu K_α radiation with Ni filters to absorb K_β radiation. An X'celerator solid-state linear position sensitive detector was used on the diffracted beam. Elevated temperatures were obtained with an Anton Paar XRK-900 furnace. All data were collected in an air atmosphere.

3.2.3 Neutron diffraction

Time-of-flight neutron diffraction data were collected at room temperature on the General Purpose Powder Diffractometer (GPPD) at the Intense Pulsed Neutron Source (IPNS) in Argonne, Illinois. Neutron diffraction has a significant advantage over X-ray diffraction for studying these materials. X-rays scatter from the electron cloud of an atom. Atomic scattering factors for X-rays go as the number of electrons, and therefore as the atomic number (Z). Several atoms of interest, Mg, Al and Si, have similar atomic numbers (12, 13 and 14, respectively), making them difficult to distinguish using X-rays. However, neutrons scatter from the nucleus of an atom. Neutron bound coherent scattering lengths (b_c) are random with the atomic number, as seen in Table 3.2. Therefore, neutron diffraction should allow the Mg^{2+}, Al^{3+} and Si^{4+} ions to be more clearly distinguished. However, few neutron sources exist, and beam time is not readily available.

Table 3.2 Bound coherent scattering lengths and atomic numbers of selected elements [53].

atom	b_c (fm)	Z
Ba	5.07	56
Ti	-3.438	22
Si	4.1491	14
Al	3.449	13
Mg	5.375	12
O	5.803	8

3.3 Diffraction Data Analysis

3.3.1 Rietveld refinement method

All diffraction data were analyzed using the Rietveld refinement method. In this method, developed by H. M. Rietveld in 1969 [54], a pattern is calculated from multiple instrumental and atomic parameters. The calculated pattern is compared to the experimental pattern using a least-squares calculation, the parameters are adjusted, and a new pattern is calculated. The procedure is then repeated until each parameter converges onto a steady value. The Rietveld method is a structural refinement method, not an ab-initio structural solution method.

3.3.2 GSAS computer program

Rietveld refinements were conducted using the General Structure Analysis System (GSAS) computer program [55] with the EPXGUI graphical user interface [56]. The reported errors are based upon estimated standard deviation values as provided by GSAS. Diffraction patterns were refined using a shifted Chebyschev background function and a pseudo-Voight profile function, which is a combination of Lorenztian and Gaussian peak shape functions. The parameters refined were: background, scale, lattice parameters, atom positions, isotropic thermal parameters, and multiple profile parameters, namely the Cagliotti instrumental broadening, Lorenztian Scherrer broadening, asymmetry and sample shift terms. For some samples, the March-Dollase preferred orientation function was refined for the <001> axis, as hexacelsian cleaves near perfectly along the (001) plane, leading to high preferred orientation in powder samples [57]. For neutron diffraction data, anisotropic thermal parameters were refined for the oxygen anions.

4. RESULTS AND DISCUSSION

4.1 Synthesis Method Comparison

4.1.1 Solid-state synthesis

Initially, samples were synthesized using a traditional solid-state synthesis method. Stoichiometric amounts of $BaCO_3$, Al_2O_3, SiO_2, MgO and TiO_2 were mixed and fired in multiple steps of increasing temperature (see section 3.1 for details). X-ray diffraction patterns were taken after some heating steps to track the phase changes occurring in the samples.

For the pure sample with no MgO or TiO_2, monoclinic celsian and hexacelsian were present after heating at 1350°C. Though celsian is the equilibrium phase at that temperature, the formation of hexacelsian as a metastable phase in this region has been previously reported [3, 6, 35]. After heating at 1500°C, only celsian was present, as expected. After heating at 1600°C, in the hexacelsian equilibrium region, for 24 hours, a mixture of celsian and hexacelsian was found, indicating that equilibrium had not yet been reached. After heating at 1600°C for 18 hours, followed by 1650°C for 24 hours, only hexacelsian was found, indicating equilibrium had been reached.

Much difficulty was encountered in synthesizing samples with approximately 15mol% MgO and 10mol% TiO_2. The first sample melted unexpectedly when the temperature was raised from 1350 to 1650°C and was lost. The second melted when the temperature was raised from 1350 to 1500°C. The third fused to the alumina boat between heating at 1440 and 1460°C. The fourth sample, that upon which diffraction data has been collected, was slowly increased in steps of 10° each from 1400 to 1460°C. It was noted that melting of the sample was observed when heating at 1450°C, but not

when heating at 1440°C. The (qualitative) amount of melting was larger when heating at 1460°C than when heating at 1450°C. X-ray diffraction data taken after heating at 1450°C indicated that the sample was celsian with unidentified secondary phase peaks, as seen in Figure 4.1. Several candidates were identified including enstatite ($MgSiO_3$, previously reported by Beall et al. [21]), karrooite ($MgTi_2O_5$, previously reported by Beall et al. [21] and Rawn et al. [22]), forsterite (Mg_2SiO_4, previously reported by Rawn et al. [22]), barium aluminate ($BaAl_2O_4$, previously reported by Colomban et al. [30]), sanbornite ($BaSi_2O_5$) and $Ba_2Si_3O_8$. The intensity of the highest intensity secondary phase peak (at 2θ=18.002°) relative to the highest intensity primary phase peak (the $(\bar{2}20)$ peak at 2θ=26.601°) was 39. Further synthesis of this sample was conducted using the melt glass crystallization method, as discussed in section 4.1.3 below.

For the sample with approximately 10mol% MgO and 6.67mol% TiO_2, celsian and the same unidentified secondary phase seen in the sample with 15mol% MgO and 10mol% TiO_2 were present after heating at 1350°C. The intensity of the highest secondary phase peak (2θ=18.002°) relative to the $(\bar{2}20)$ celsian peak was 32. After heating at 1500°C, the relative intensity of the secondary phase peak was 5.9. After heating at 1600°C, the sample was celsian with no visible trace of the secondary phase. Figure 4.2 compares the diffraction patterns taken after heating at 1350, 1500 and 1600ºC. After heating at 1620°C, the sample was a mixture of hexacelsian and celsian. The sample was not fully converted to hexacelsian until heated at 1635°C for 24 hours. A trace of the secondary phase was present.

For the sample, with approximately 7.5mol% MgO and 5mol% TiO_2, celsian and the same unidentified secondary phase seen in the previous two samples were present after heating at 1350°C for 24 hours. The relative intensity of the highest secondary phase peak (2θ~18º) was 28. The relative intensity of the same peak did not change after heating at 1350°C for an additional 24 hours, but increased significantly after heating at 1350ºC for 60 hours, as seen in Figure 4.3. After heating at 1620°C, the sample was

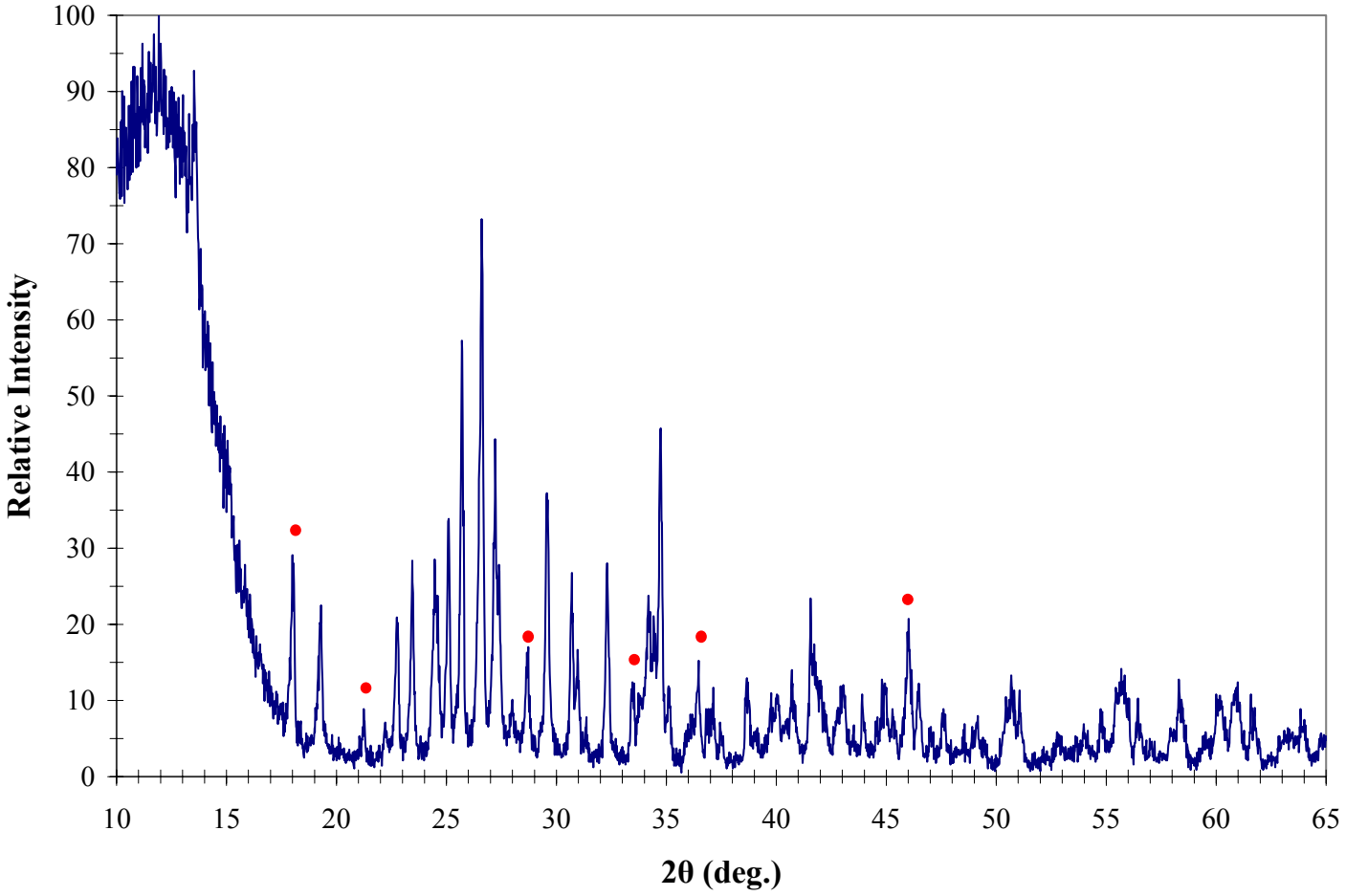

Figure 4.1 X-ray diffraction pattern of sample with 15mol% MgO and 10mol% TiO_2 after heating at 1450ºC. The primary phase is celsian. The red dots mark secondary phase peaks.

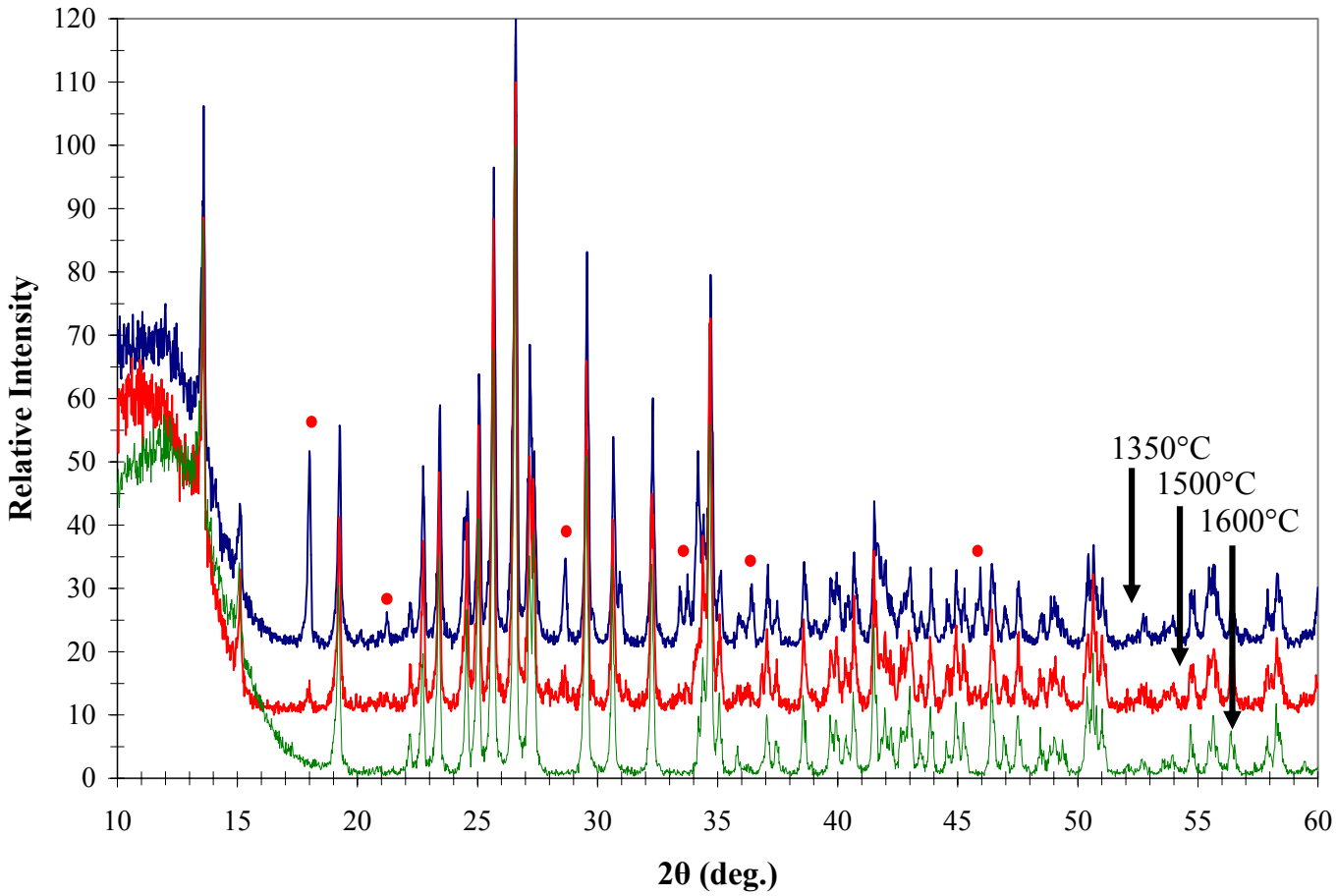

Figure 4.2 X-ray diffraction patterns of sample with 10mol% MgO and 6.67mol% TiO_2 after heating at 1350, 1500 and 1600ºC. The primary phase is celsian. The red dots mark secondary phase peaks.

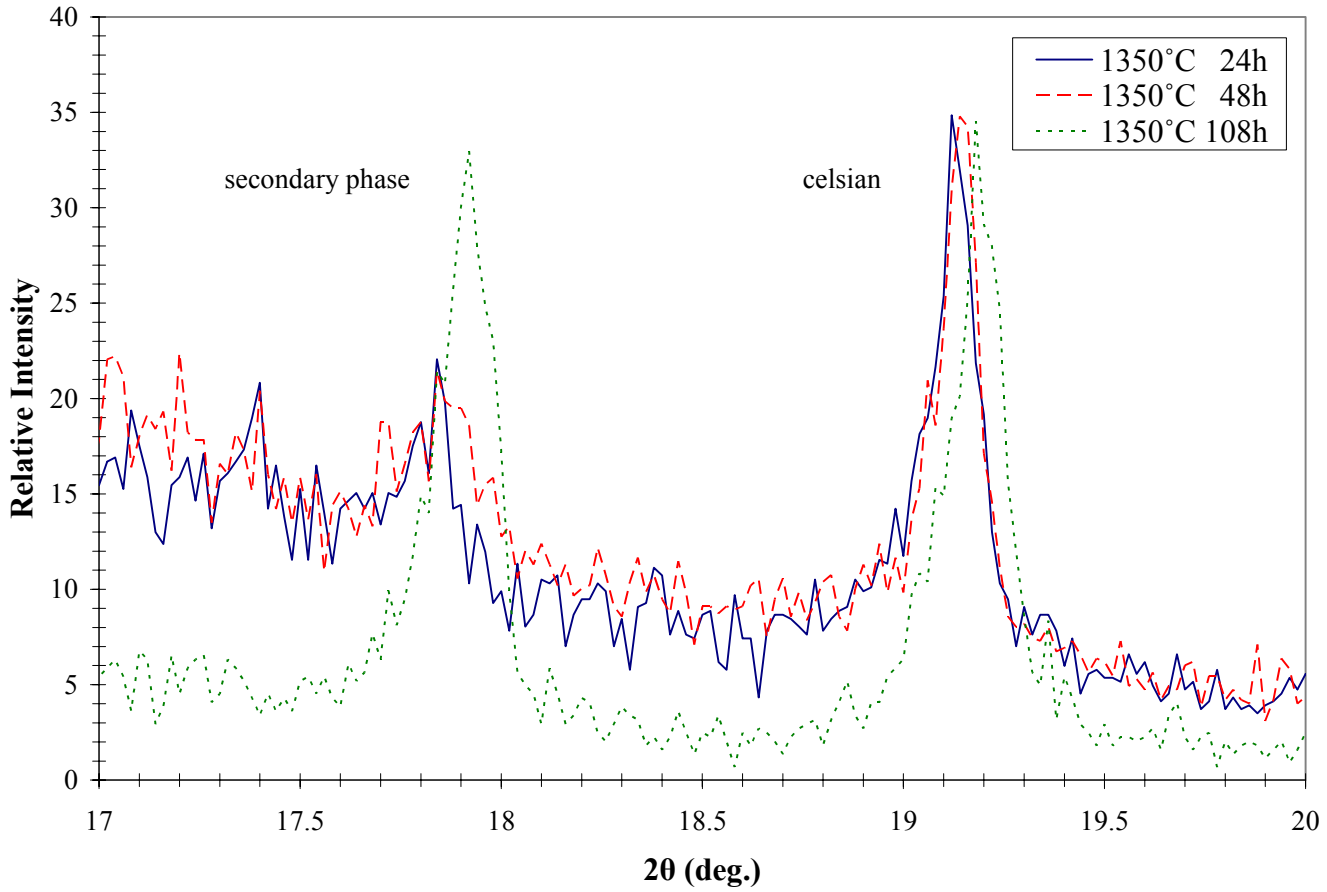

Figure 4.3 X-ray diffraction patterns of sample with 7.5mol% MgO and 5mol% TiO_2 after heating at 1350ºC for 24, 48 and 108 total hours. The primary phase is celsian.

celsian with only a trace of the secondary phase. The celsian fully converted to hexacelsian when heated at 1650°C.

From the solid-state synthesis of the pure and MgO and TiO_2 substituted samples, it was verified that hexacelsian can form metastably at temperatures below its equilibrium region, as had been previously reported [3, 6, 35]. In addition the data suggests that the celsian → hexacelsian transition may be sluggish. Though the transformation temperature is 1590°C, complete conversion to hexacelsian was not found for heating at temperatures below 1635°C for 24 hours for any of the pure or substituted compositions. Indeed, for the sample with 7.5mol% MgO and 5mol% TiO_2, heating at 1620°C for 24 hours produced no evidence of hexacelsian formation. Though the celsian → hexacelsian transformation has not been previously studied, the reverse hexacelsian → celsian transformation has been previously reported to be quite sluggish [7, 17-19]. The poor kinetics of both the forward and reverse transitions suggests that a structurally independent factor may be affecting the transitions. A more thorough study would be needed to draw any concrete conclusions.

Also, it was found that the formation of secondary phases in the MgO and TiO_2 substituted samples was difficult to avoid. The secondary phase could not be identified from the solid-state experiments due to two factors: peak overlap with celsian peaks, of which there are many due to its low symmetry, and insufficient peak intensities in the hexacelsian samples, in which only traces of the secondary phase were found. The secondary phase appeared to be in equilibrium with BAS at 1350°C. At temperatures of 1500°C and above, the amount of secondary phase decreased with increasing temperature. The secondary phase caused a small amount of melting at 1450°C, but not at 1440°C. The amount of melting appeared to increase with increasing temperature. These results suggest that the as-yet unidentified secondary phase has a eutectic relationship with BAS, with a eutectic temperature around 1440 to 1450°C. Of the previously mentioned candidates for the secondary phase, the equilibrium relationships of

both the barium silicates are known; their eutectic temperatures, 1227 and 1216ºC for $BaSi_2O_5$ and $Ba_2Si_3O_8$ respectively, are below the expected range [5].

4.1.2 Multiple step solid-state synthesis

Phase development was also tracked in the sample with approximately 15mol% MgO and 10mol% TiO_2 synthesized using the two-step solid-state method outlined by Lee and Aswath [9, 33]. After the first step, i.e. firing a 1:2 molar mixture of $BaCO_3$:SiO_2 at 1150ºC for four hours, the sample was a mixture of various barium silicates. After the second step, i.e. firing the above in a 1:1 molar mixture with Al_2O_3 at 1200ºC for six hours, the sample was a mixture of hexacelsian, alumina and barium silicates. In an attempt to form more hexacelsian, the sample was heated a further two hours at 1200ºC with no appreciable effect. Approximately 15mol% MgO and 10mol% TiO_2 were added to the sample, which was then heated for four hours at 1200ºC. X-ray diffraction showed the sample to be primarily celsian, with hexacelsian also present, as seen in Figure 4.4.

4.1.3 Melt glass crystallization

As stated in section 4.1.1 above, solid-state synthesis of the sample with approximately 15mol% MgO and 10mol% TiO_2 was abandoned after it was realized that temperature increases above 1440ºC would result in melting. Synthesis was continued using the melt glass crystallization technique. After the sample was completely melted in a platinum crucible at 1650ºC and furnace cooled, the sample was crushed for X-ray powder diffraction. The sample was observed to fracture in a shard-like manner. The diffraction pattern, seen in Figure 4.5, had diffuse scattering, as well as crystalline peaks of hexacelsian and the previously unidentified secondary phase. No celsian was present, indicating that the cooling rate was sufficiently high to prevent its formation. The secondary phase peaks had sufficient intensity to allow the phase to be identified as Mg_2TiO_4. Additional, low-intensity peaks were also observed. Heating at 1000ºC for

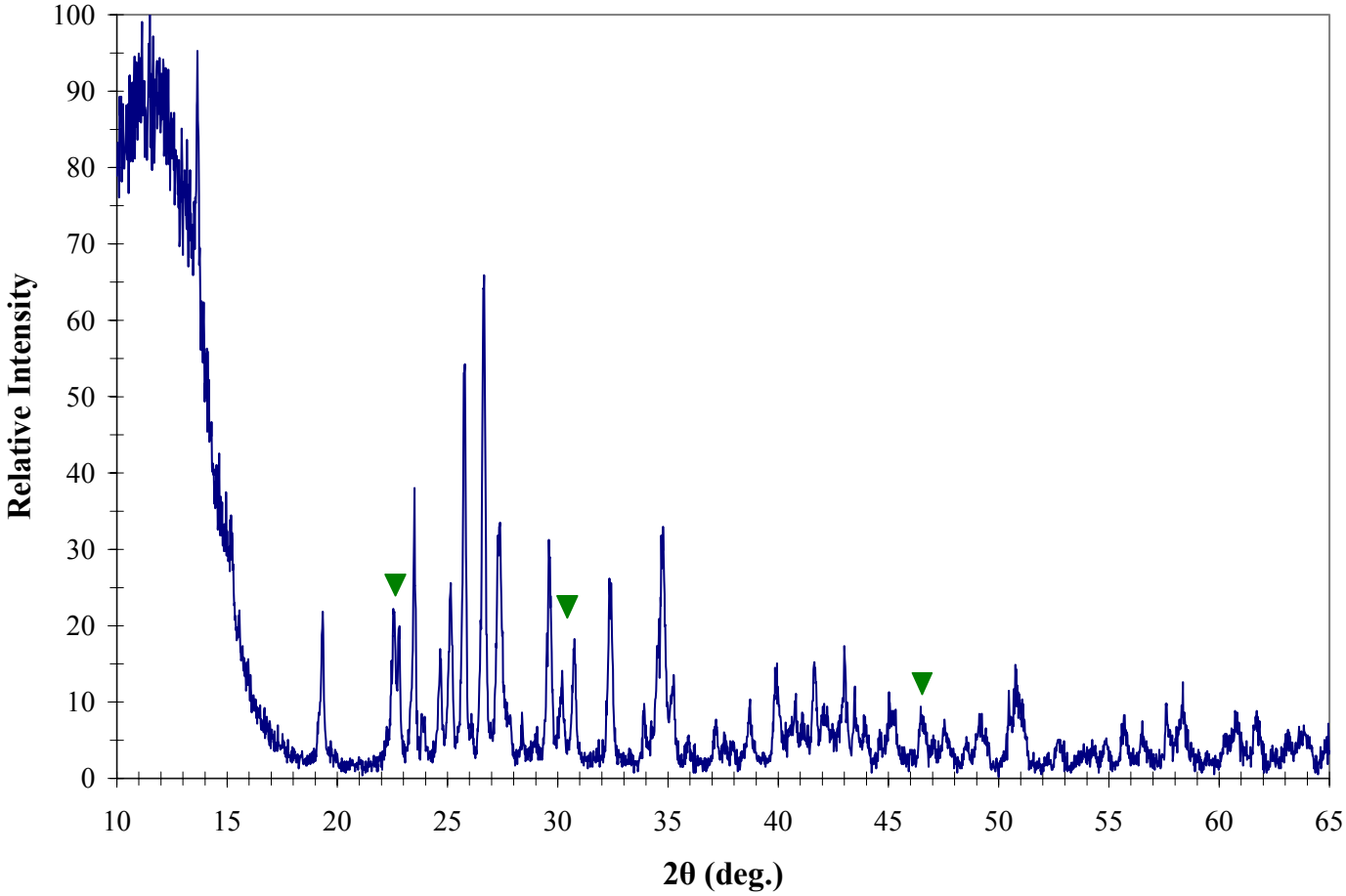

Figure 4.4 X-ray diffraction pattern of sample with 15mol% MgO and 10mol% TiO_2 synthesized using the multiple step solid-state method. The primary phase is celsian. The green triangles mark hexacelsian peaks.

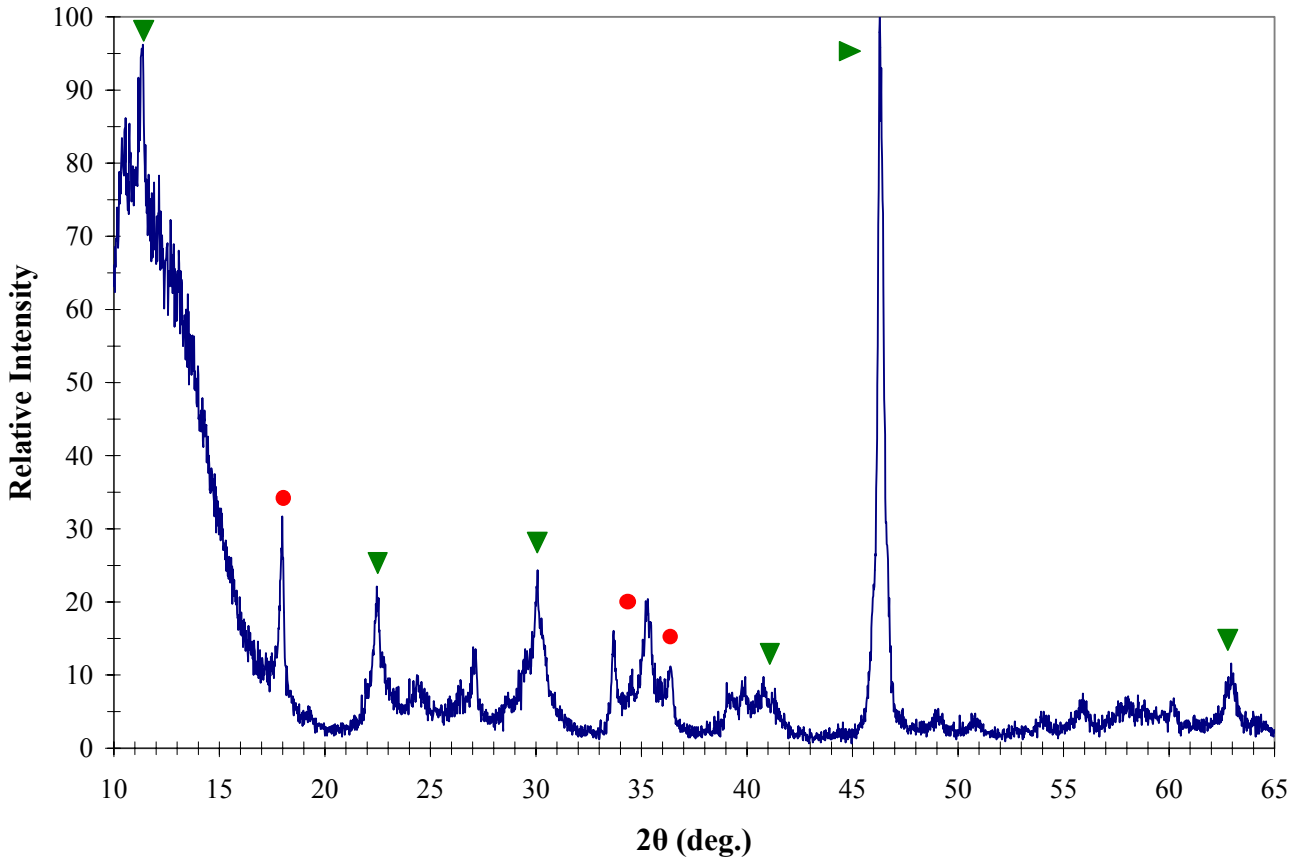

Figure 4.5 X-ray diffraction pattern of sample with 15mol% MgO and 10mol% TiO_2 after melting. The green triangles mark hexacelsian peaks. The red dots mark secondary phase peaks.

fours hours, and then a further two hours at 1000ºC and nine hours at 1100ºC did not significantly affect the diffuse or amorphous scattering, as seen in Figure 4.6. (The amorphous scattering from the sample is concealed in Figure 4.5 due to amorphous scattering from the sample holder.)

A sample with approximately 5mol% MgO and 3mol% TiO_2 was also synthesized using the melt glass crystallization technique. Heating the sample up to 1350ºC resulted in celsian with a small amount of the secondary Mg_2TiO_4 phase. The sample was further heated up to 1500ºC before being completely melted at 1650ºC and furnace cooled. Grains large enough to be visible to the naked eye (approximately 1mm in diameter) were observed along the edges of the sample. The sample was observed to fracture in a flake-like manner. The X-ray diffraction pattern, seen in Figure 4.7, showed the sample to be a mixture of hexacelsian and celsian, unlike the previous melt glass sample, which contained no celsian. The pattern also exhibited some amount of diffuse scattering.

Larger amounts of MgO and TiO_2 additions appear to favor the formation of hexacelsian over celsian, though the mechanism is unknown. However, other researchers [12, 19] have reported that substitutions and vacancies favor the hexacelsian → celsian transformation due to increases in the hexacelsian energy.

4.1.4 Sol-gel synthesis

Room-temperature X-ray diffraction was also used to study the synthesis of a pure sample using the sol-gel method. Following gelation, the gel was dried for two hours at 115°C and X-ray diffraction data was collected. The sample was determined to be primary barium acetate, indicating that the sample was not yet completely dried. The sample was dried further at 120°C for two to three days. The powder was then heated at 600°C for 24 hours, and then at 800°C for 24 hours. X-ray diffraction showed the sample to be a mixture of barium aluminate ($BaAl_2O_4$) and two barium silicates ($BaSiO_3$ and $BaSi_2O_5$) with some diffuse scattering.

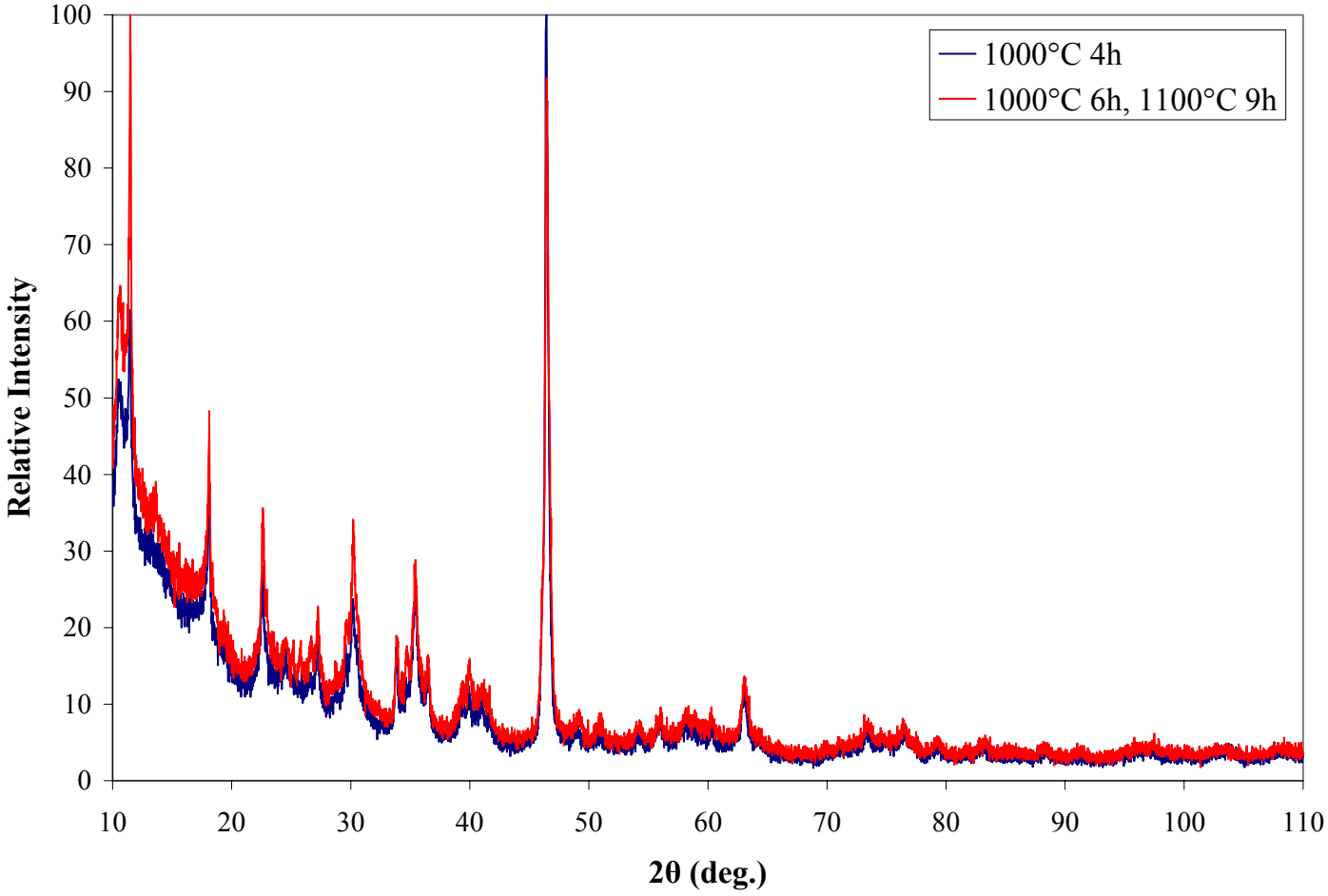

Figure 4.6 X-ray diffraction patterns of sample with 15mol% MgO and 10mol% TiO_2 after melting and crystallization at 1000 and 1100ºC. The pattern exhibits diffuse scattering at low angles.

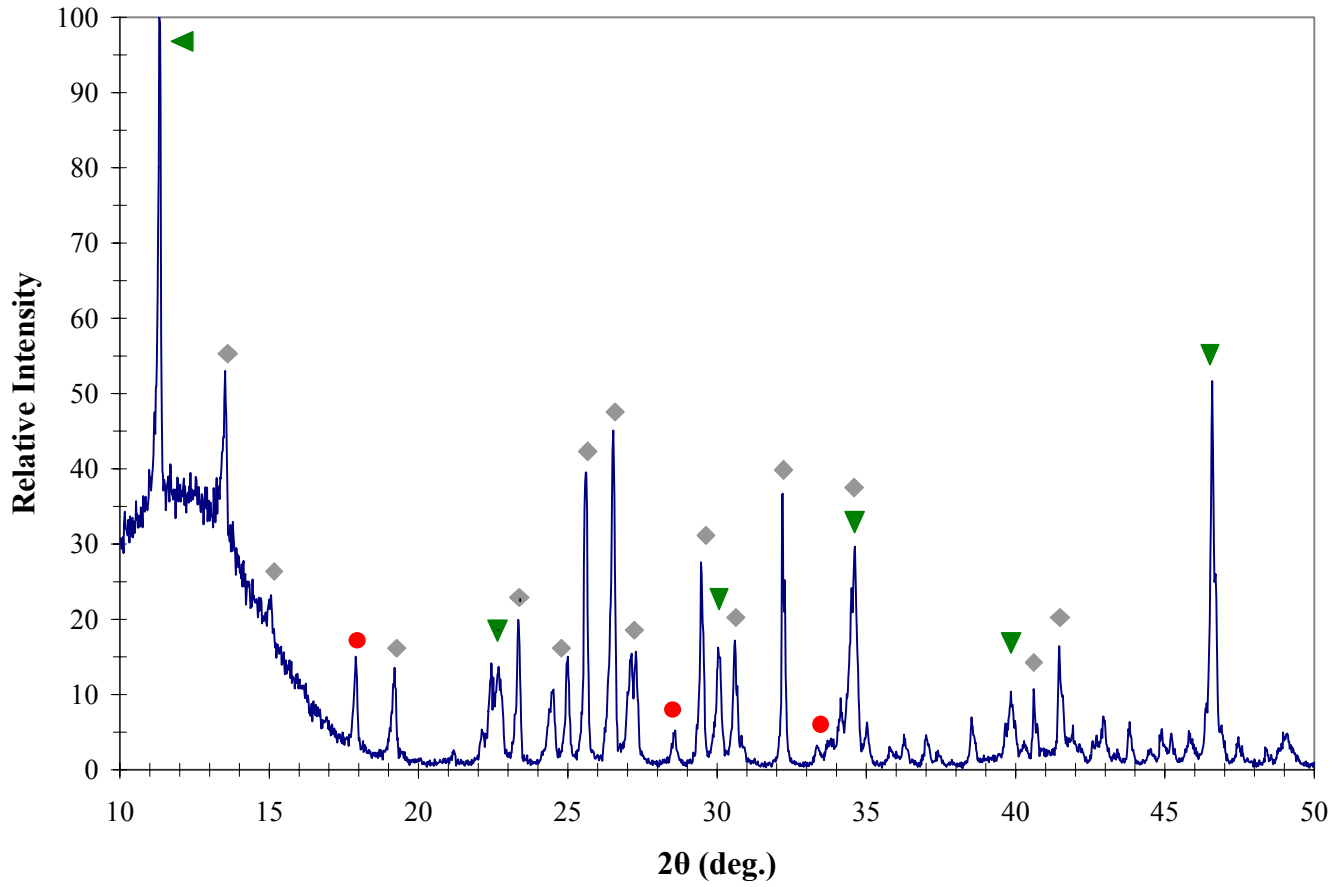

Figure 4.7 X-ray diffraction pattern of sample with 5mol% MgO and 3mol% TiO_2 after melting. The green triangles mark hexacelsian peaks, the grey diamonds celsian peaks, and the red dots secondary phase peaks.

4.2 High-Temperature X-Ray Diffraction

4.2.1 Refined lattice parameters

High-temperature X-ray diffraction data were collected to investigate the α↔β phase transition of the pure sample and substituted samples with 15mol%MgO and 10mol% TiO_2, 10mol%MgO and 6.67mol% TiO_2, and 7.5mol% MgO and 5mol% TiO_2. Diffraction patterns were collected from 25ºC to 400-425ºC in intervals of 25ºC. The lattice parameters and derived volume, plotted in Figures 4.8-4.10, were determined from Rietveld refinements using the *P-3* space group. Diffraction data of the melt glass crystallization sample with approximately 15mol% MgO and 10mol% TiO_2 were unable to be refined due to the large amount of diffuse scattering. A clear discontinuity in the lattice parameters near 300ºC, indicating the presence of the α↔β transition, is observed for all compositions for which refined lattice parameters were obtained. The discontinuity is larger in the *a*-axis than in the *c*-axis.

Figure 4.11 plots lattice parameters against composition at 25 and 350ºC, i.e. in the α- and β-phases, respectively. MgO and TiO_2 additions of 7.5 and 5mol%, respectively, increased the *a*-axis by more than 0.02 Å in both the α- and β-phases. Increasing the additions to 10 and 6.67mol%, respectively, caused no significant change in the *a*-axis of the α-phase, though in the β-phase it slightly decreased the *a*-axis. For the *c*-axis, a V-shaped relationship with composition is observed. For both the α- and β-phases, the *c*-axis of the sample with 7.5mol% MgO and 5mol% TiO_2 is significantly smaller than for the other compositions.

Figure 4.12 plots unit cell volume against composition at 25 and 350ºC, i.e. in the α- and β-phases. Additions of 7.5mol% MgO and 5mol% TiO_2 increased the unit cell volume by approximately 0.13 $Å^3$ in the α-phase and 0.23 $Å^3$ in the β-phase. Further additions of 10mol% MgO and 6.67mol% TiO_2 had no significant impact on the unit cell volume in either the α- or β-phases.

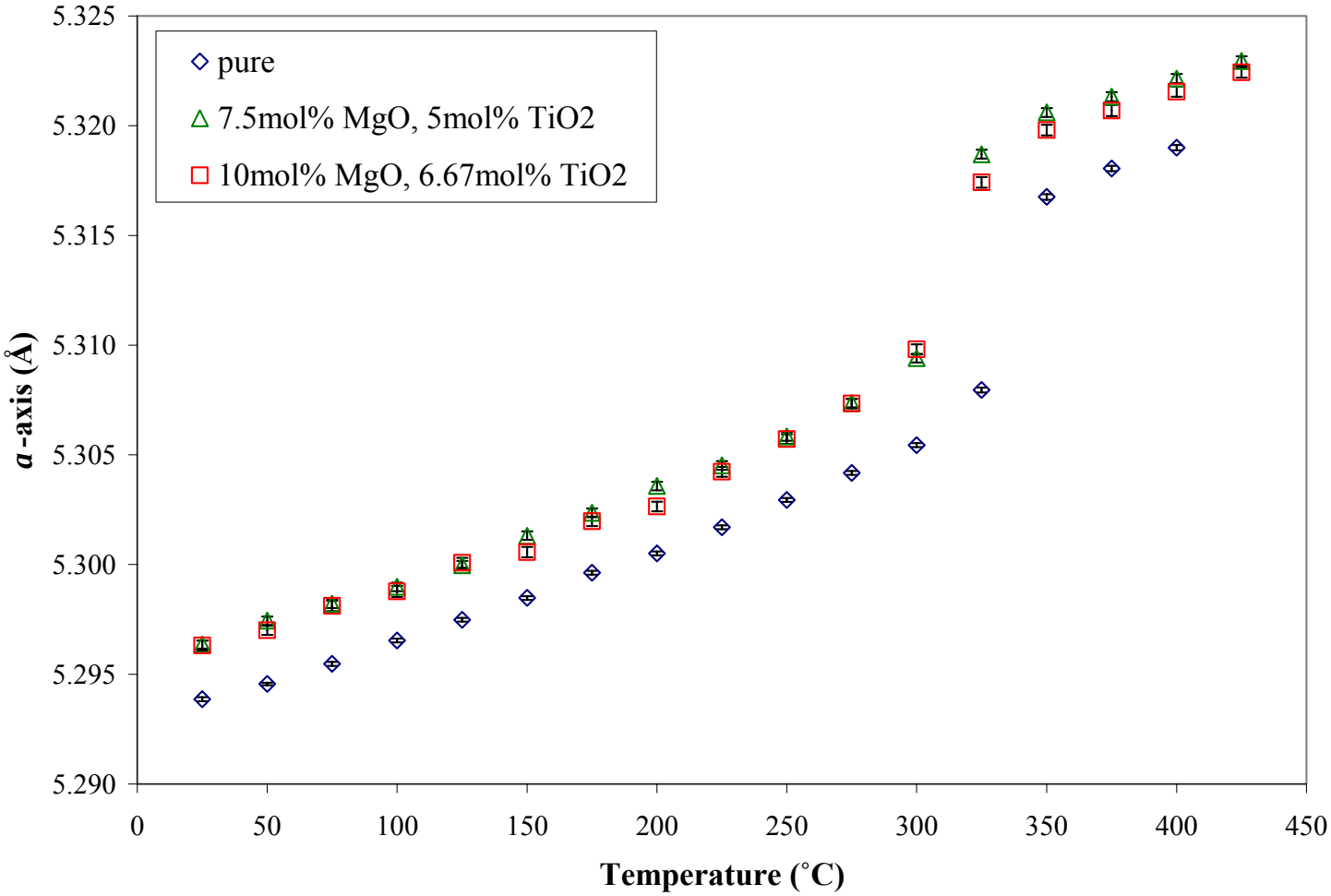

Figure 4.8 Refined lattice parameter (*a*-axis) as a function of temperature for three different compositions.

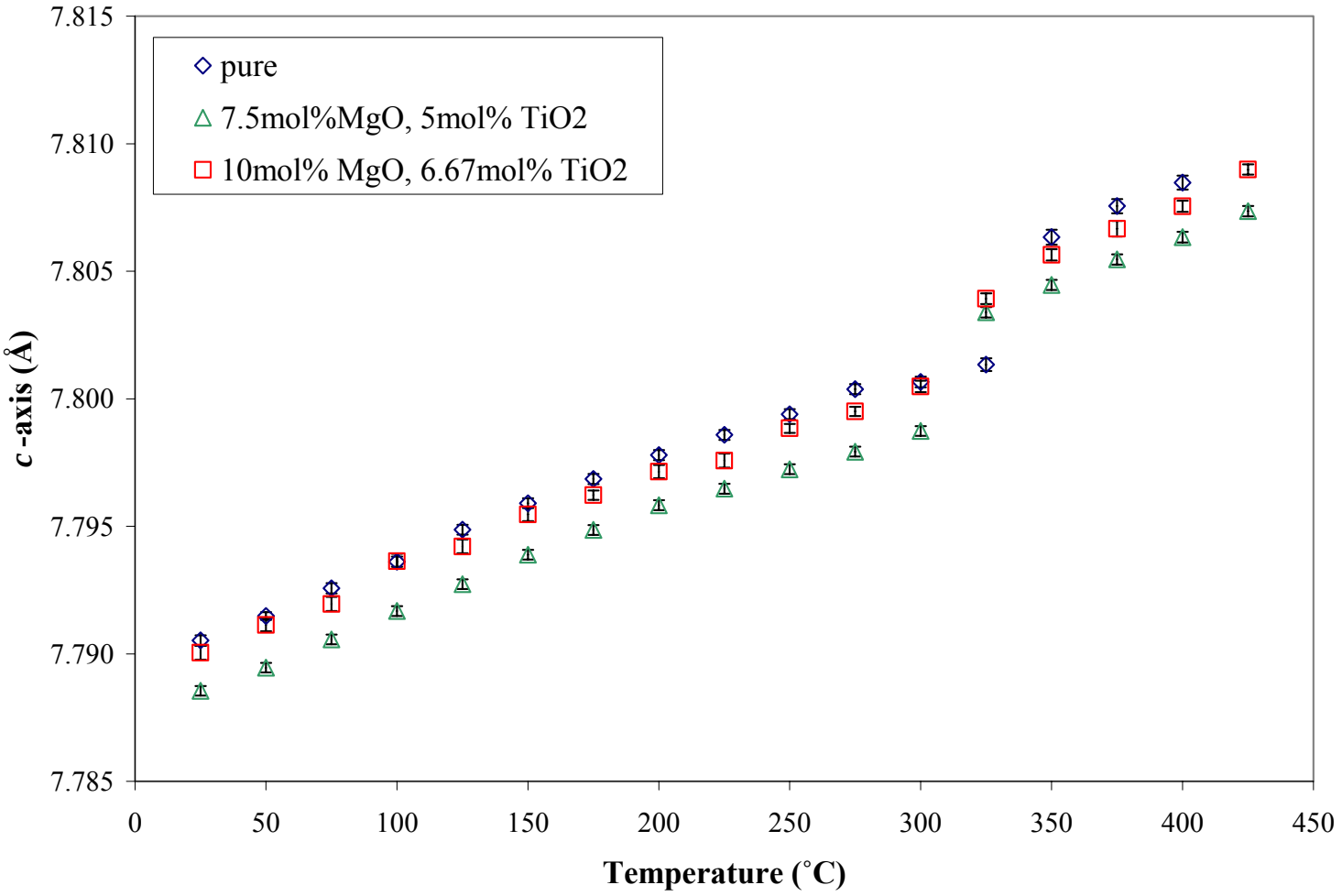

Figure 4.9 Refined lattice parameter (*c*-axis) as a function of temperature for three different compositions.

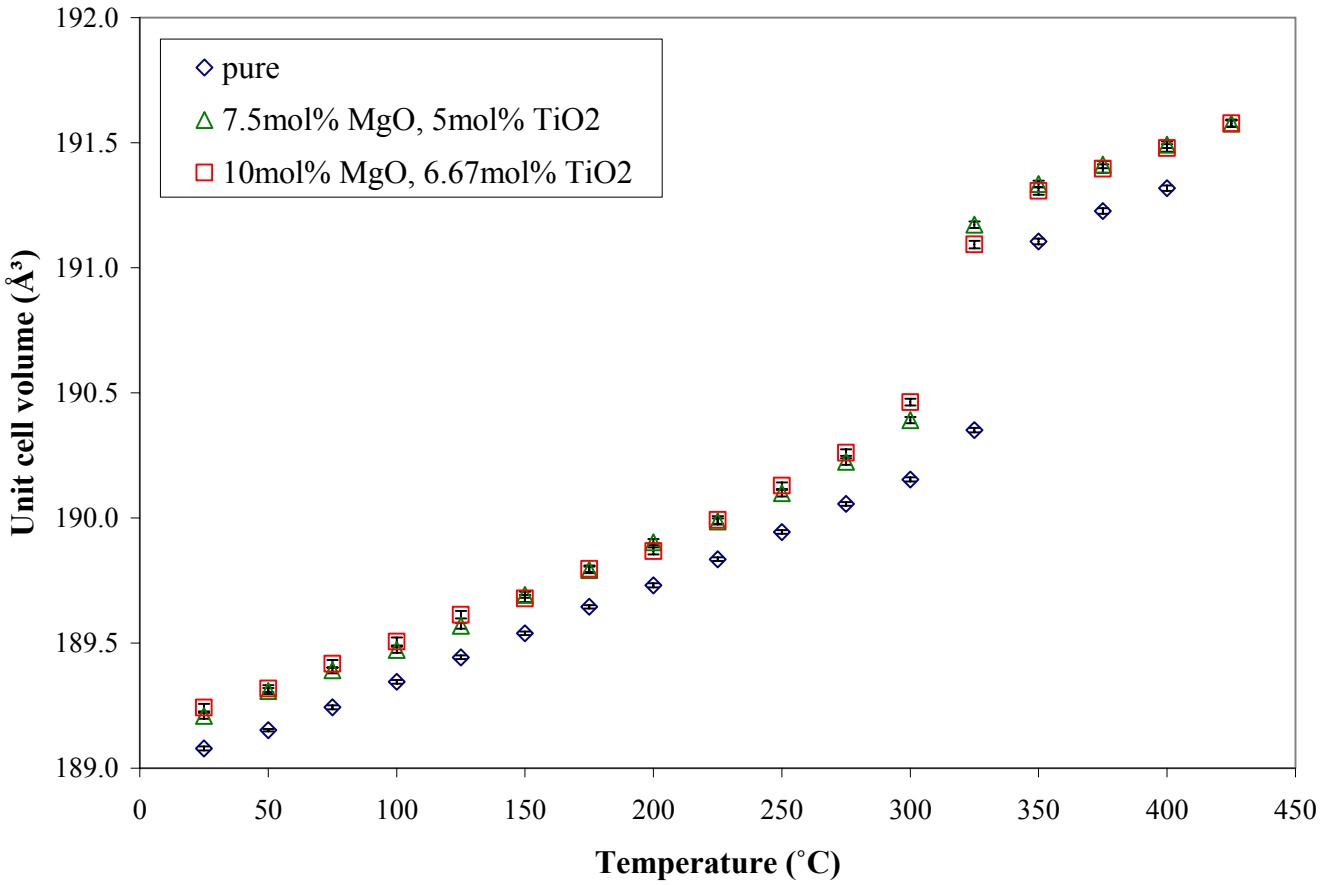

Figure 4.10 Unit cell volume derived from refined lattice parameters as a function of temperature for three different compositions.

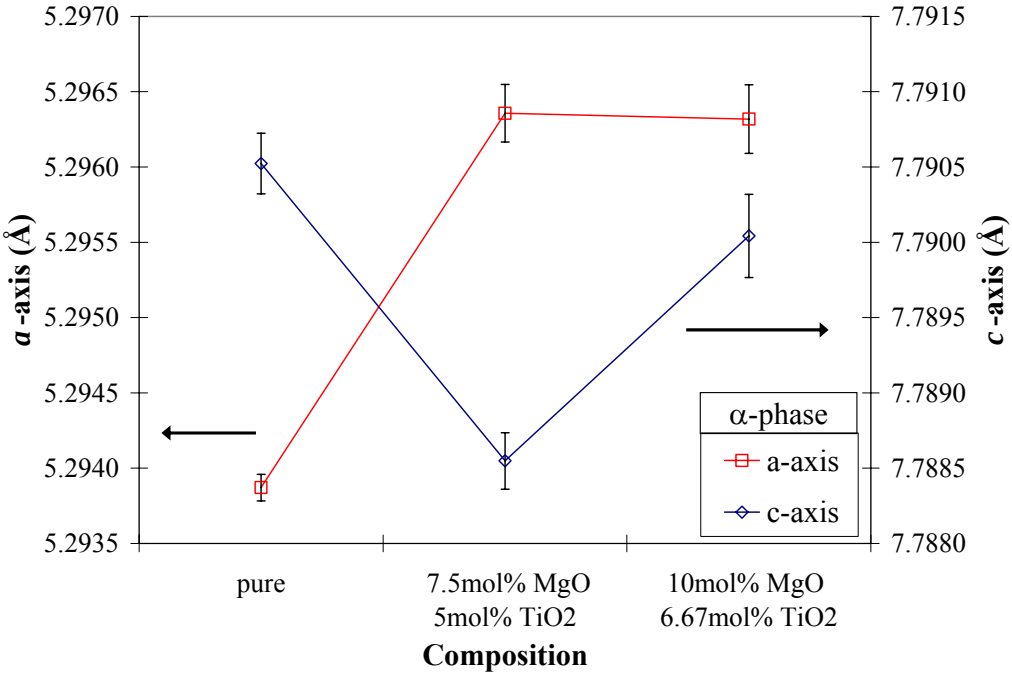

(a)

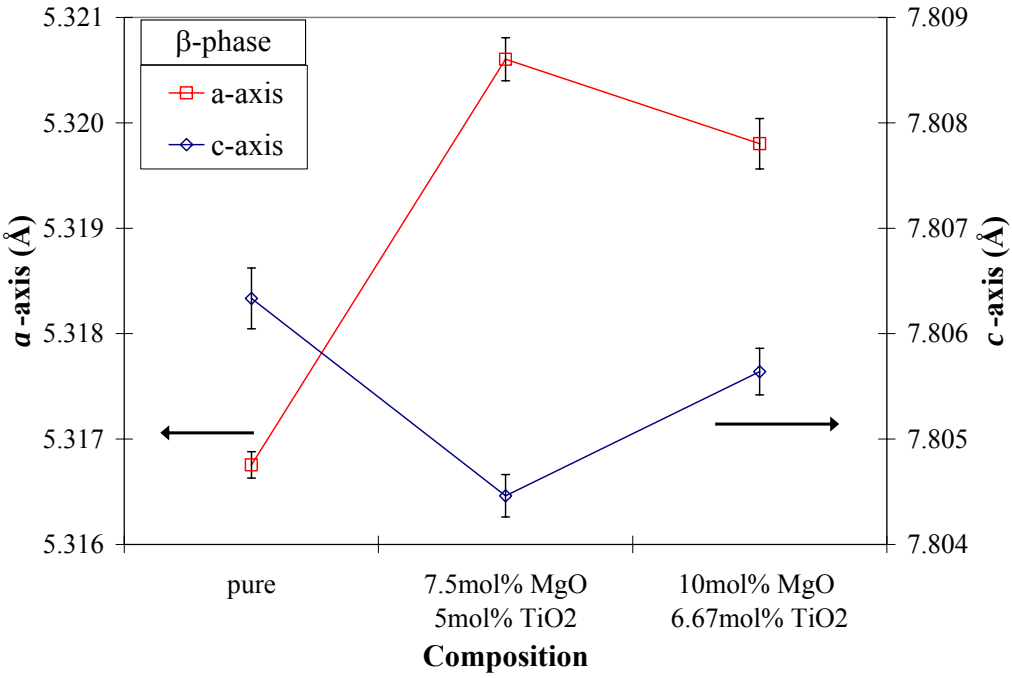

(b)

Figure 4.11 Refined lattice parameters against composition at (a) 25ºC and (b) 325ºC.

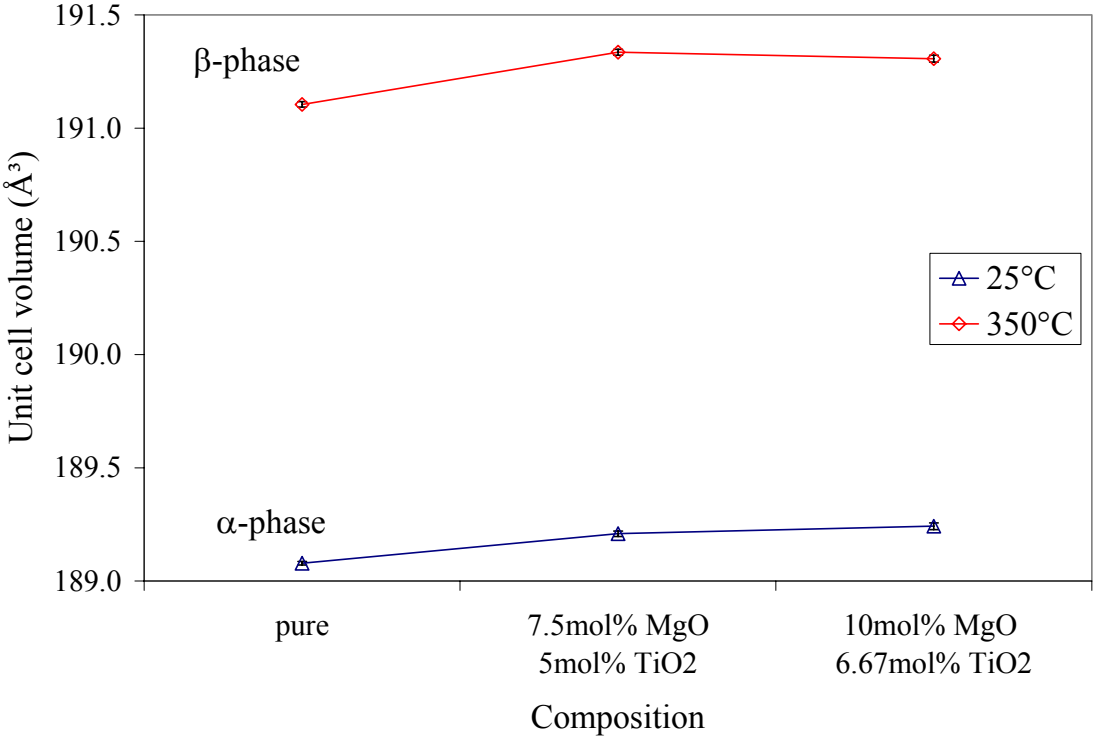

Figure 4.12 Unit cell volume against composition at 25 and 350ºC.

4.2.2 Presence of α↔β phase transition

Rawn et al. [22] have reported that additions in the amounts of 15mol% MgO and 10mol% TiO_2 suppressed the α↔β transition in a melt-glass crystallized sample, such that no discontinuity in lattice parameters was visible. Refined lattice parameters were not able to be obtained for the sample of the current work with the same composition. However, close observation of peak positions revealed no discontinuity in peak position, as was seen with the pure sample. Therefore, it may be concluded that the α↔β transition was suppressed by the addition of 15mol% MgO and 10mol% TiO_2 to hexacelsian when using melt glass crystallization synthesis.

In U.S. patent #5,910,459 ("Glass-ceramic containing a stabilized hexacelsian crystal structure") [21], Beall et al. reported that the addition of 20mol% MgO, 9mol% TiO_2, and 1mol% ZnO, as well as the addition of 29mol% MgO, 9mol% TiO_2, and 1mol% ZnO, stabilized the thermal expansion of melt-glass crystallized hexacelsian, as determined by dilatometry. The ranges claimed in the patent to stabilize the thermal expansion of hexacelsian were as follows: 5-35mol% BaO, 5-25mol% Al_2O_3, 35-55mol% SiO_2, 5-25mol% MgO, 6-14mol% TiO_2, 0-10mol% ZnO and 0-8mol% ZrO. The claims of the patent conflict with the absence of a stabilized thermal expansion in the sample with approximately 10mol% MgO and 6.67mol% TiO_2, as determined by X-ray diffraction. The discrepancy could be due to the presence of a secondary phase, enstatite ($MgSiO_3$). (The thermal expansion as determined by X-ray diffraction would not include the effect of secondary phases, which would be visible in dilatometric measurements.) However, Beall et al. also found stabilized thermal expansion of a sample with little to no enstatite, indicating that secondary phases do not play a large role in stabilizing the thermal expansion.

The α↔β transition temperature was found to be weakly dependent on the composition. The pure sample underwent the α↔β transition between 325 and 350ºC, while the substituted samples underwent the α↔β transition between 300 and 325ºC. The decrease

in transition temperature could be due to non-stoichiometry of the hexacelsian, induced by the MgO and TiO_2 additions. Müller [26] speculated that changes in the stoichiometry of hexacelsian can significantly lower the α↔β transition temperature, even to the extent of lowering the transition temperature below room temperature.

4.2.3 Thermal expansion coefficients

High-temperature X-ray diffraction data were also used to investigate the thermal expansion of pure and substituted hexacelsian. Linear and volumetric thermal expansion is governed by Equations 1 and 2 below, respectively, where L and V are the length and volume, L_0 and V_0 are the initial length and volume, the coefficients α and β are the linear and volumetric thermal expansion coefficients, and T is the temperature [58].

$$\frac{\delta L}{L_0} = \alpha * \delta T \tag{1}$$

$$\frac{\delta V}{V_0} = \beta * \delta T \tag{2}$$

Therefore, the thermal expansion coefficients may be obtained from the slopes of plots of the fractional change in length (or volume) versus temperature, seen in Figures 4.13 - 4.15. The thermal expansion coefficients of the α-phase were calculated from linear fits of the data and are found in Table 4.1.

The thermal expansion coefficients of α-hexacelsian are plotted as a function of composition in Figure 4.16. Overall, the thermal expansion coefficients increased with increasing amounts of additions. However, on a smaller scale, a more complex relationship was observed for the *a*-axis and volume thermal expansion coefficients. These thermal expansion coefficients are larger for the sample with 7.5mol% MgO and

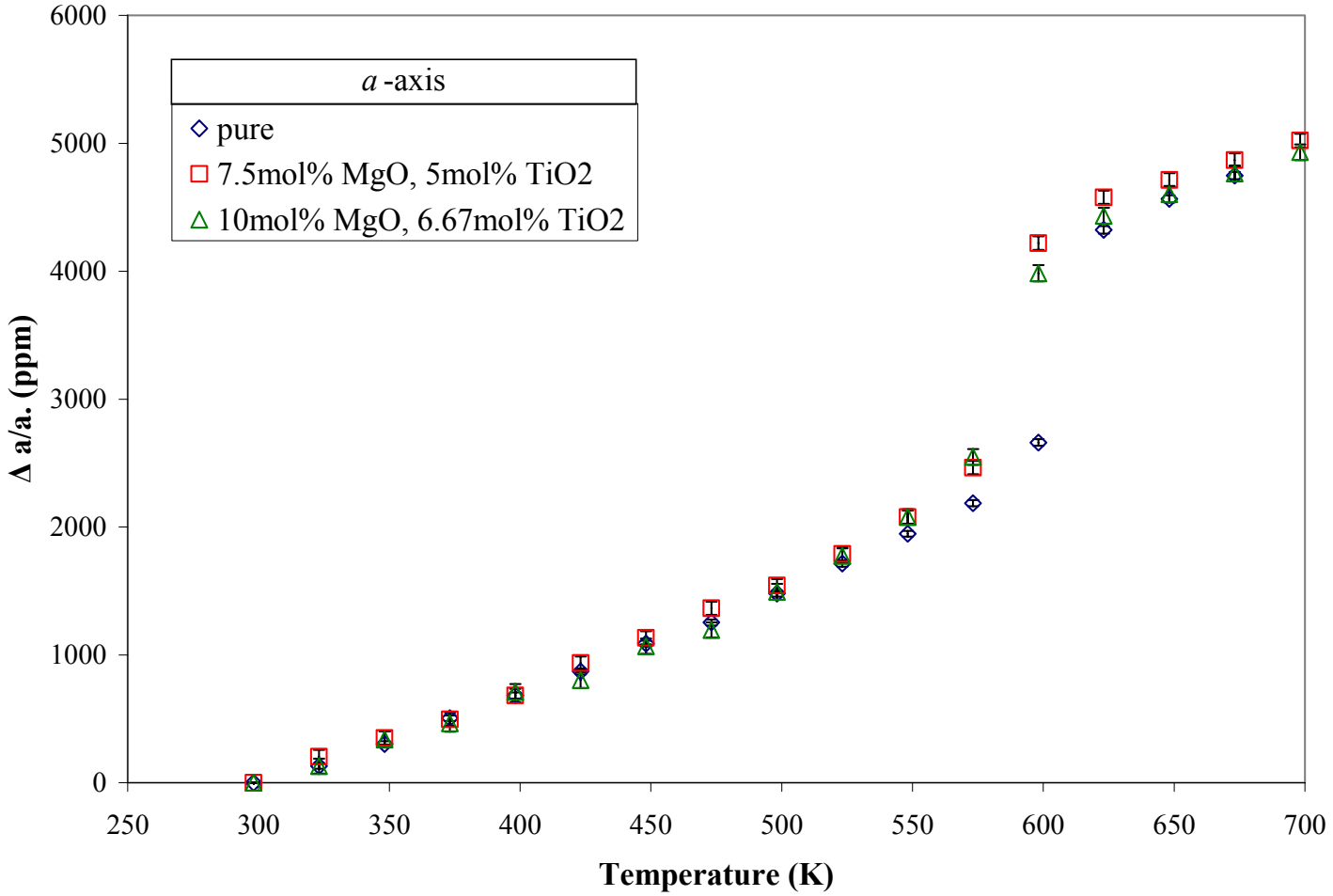

Figure 4.13 Fractional change in lattice parameter (*a*-axis) as a function of temperature for three different compositions.

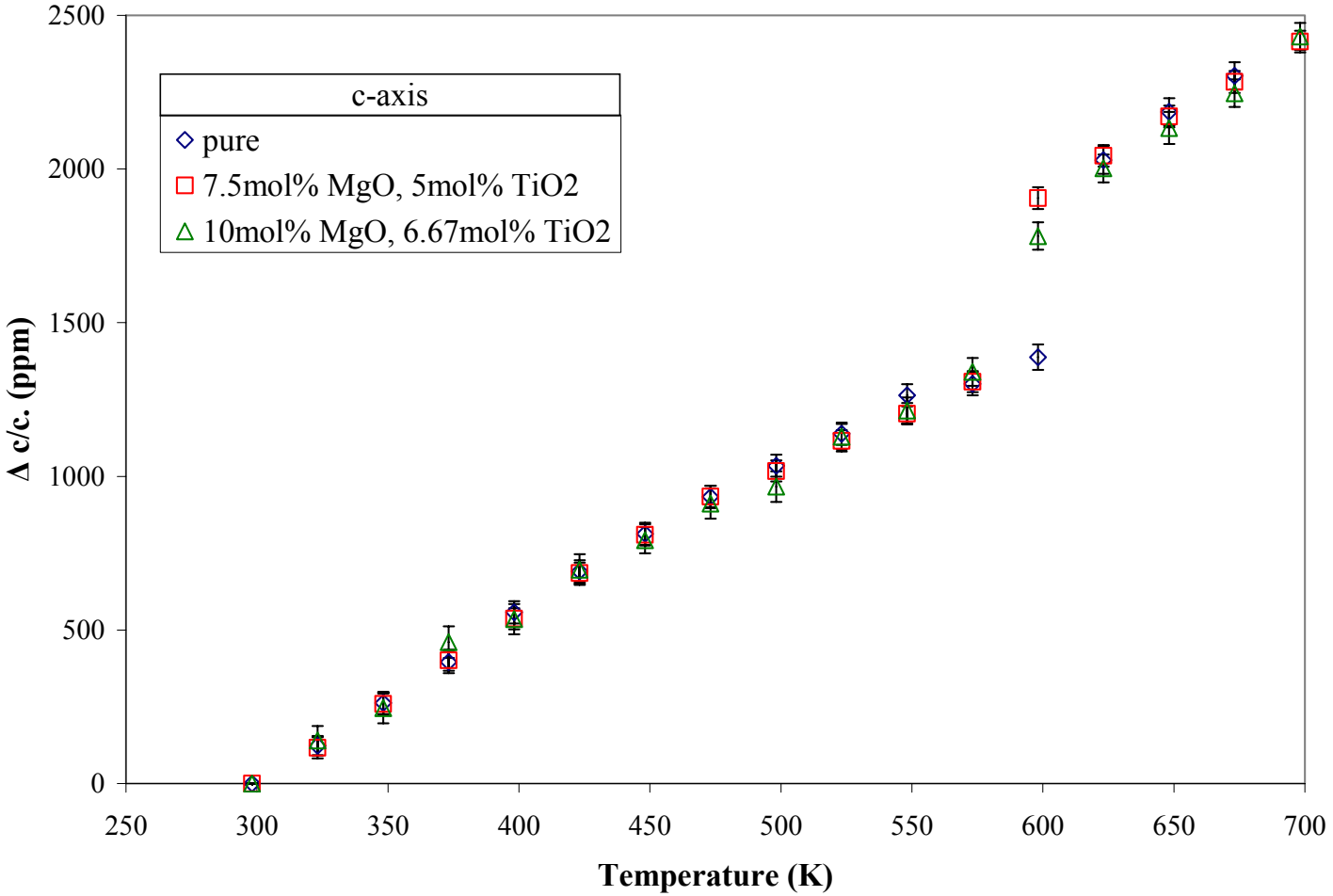

Figure 4.14 Fractional change in lattice parameter (*c*-axis) as a function of temperature for three different compositions.

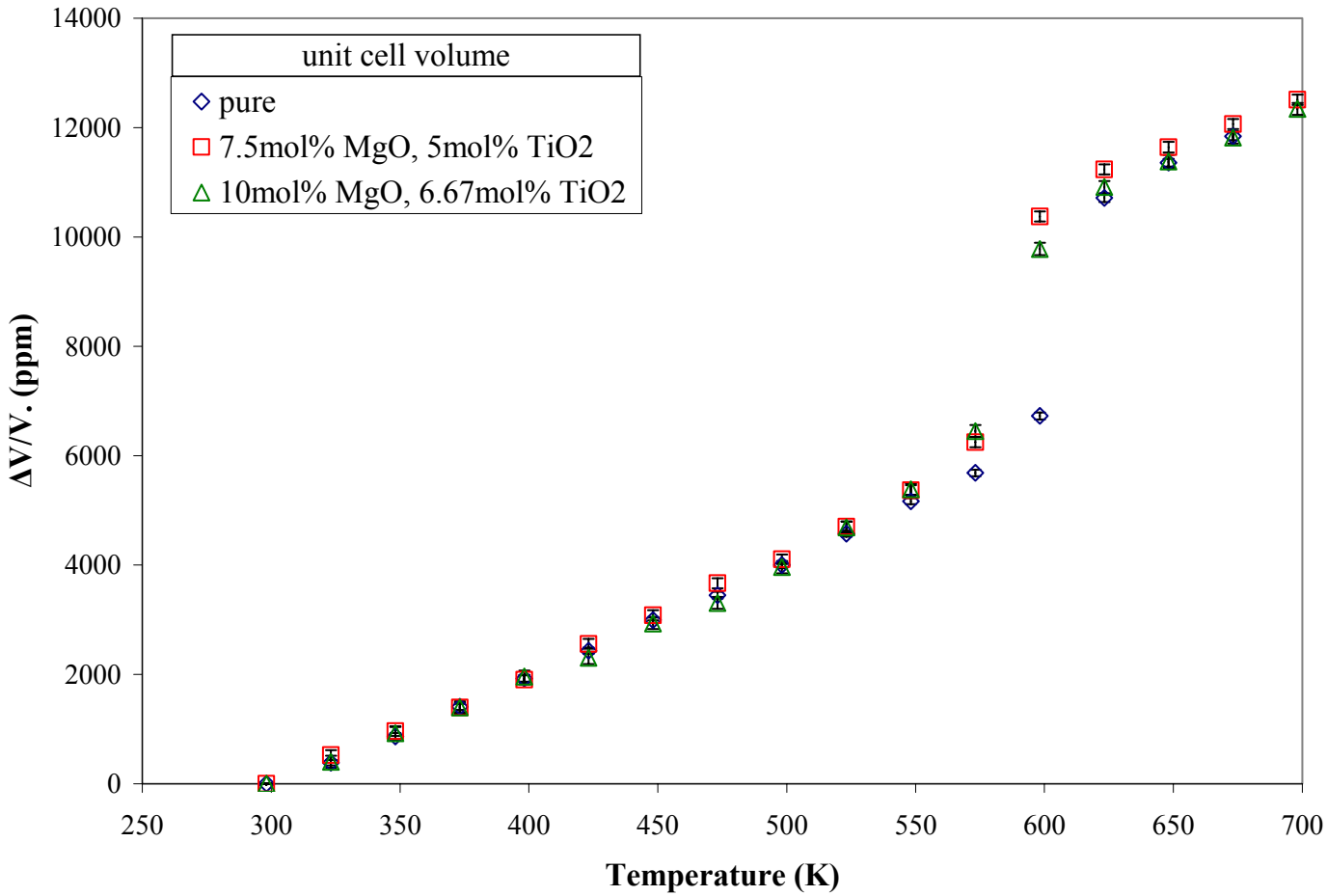

Figure 4.15 Fractional change in unit cell volume as a function of temperature for three different compositions.

Table 4.1 Thermal expansion coefficients for α-hexacelsian.

Composition (mol%)		**Thermal Expansion Coefficient (ppm / K)**		
MgO	**TiO_2**	***a*-axis**	***c*-axis**	**volume**
0	0	7.837	4.988	20.07
7.5	5	8.101	5.013	21.25
10	6.67	7.951	5.024	20.97

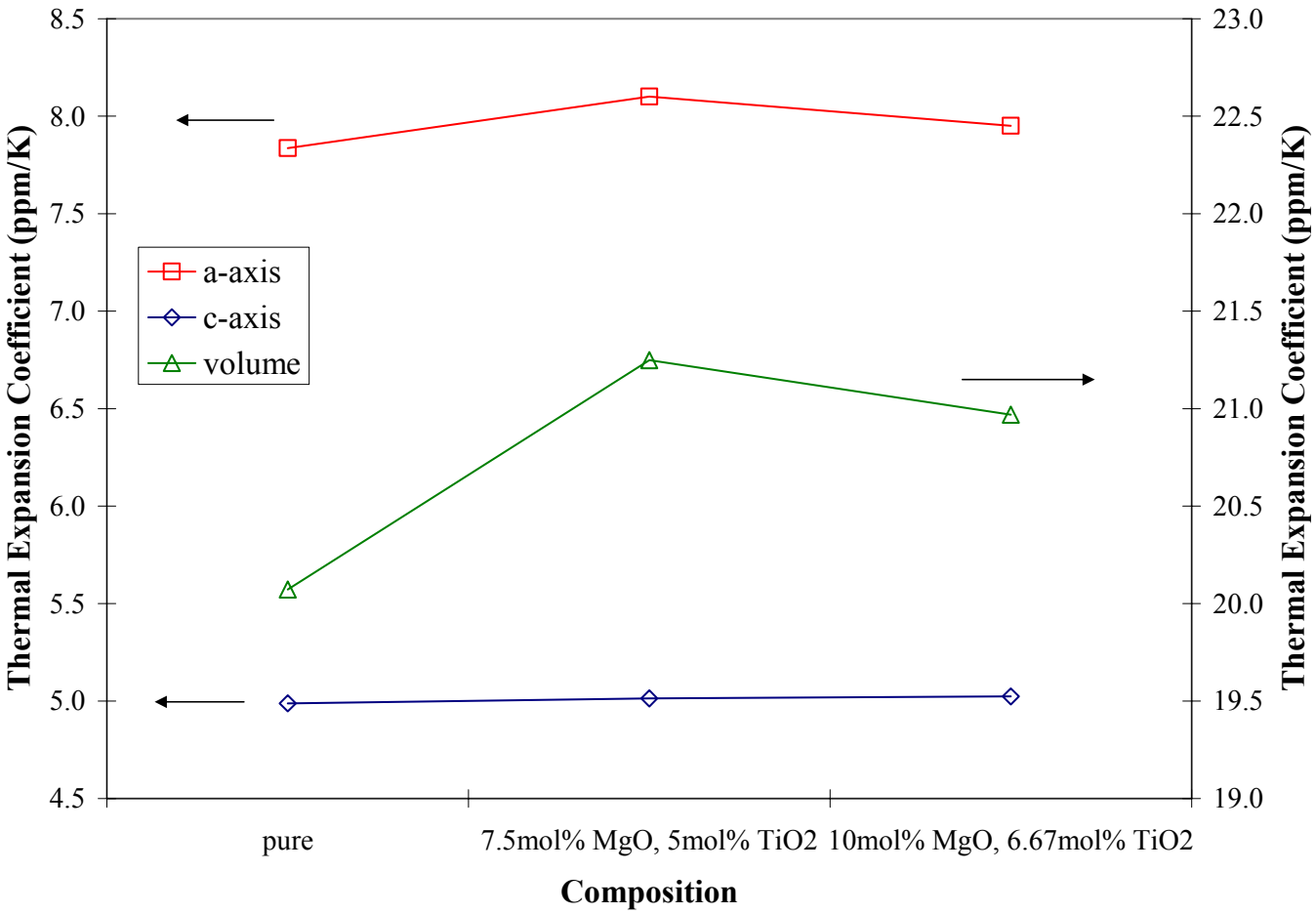

Figure 4.16 Thermal expansion coefficients of α-hexacelsian for three different compositions.

5mol% TiO_2 than for the other compositions. This result mirrors that concerning the lattice parameters, previously discussed in section 4.2.1.

The calculated thermal expansion coefficients are lower than those previously reported by Kremenović, et al. [12] for zeolite-derived hexacelsian. For zeolite A derived α-hexacelsian, the reported thermal expansion coefficients are 10.5, 8.3, and 32 ppm/K for the *a*-axis, *c*-axis and volume, respectively. The coefficients for zeolite X derived hexacelsian are similar: 10.3, 9.3 and 30.7 ppm/K. These previously reported thermal expansion coefficient values are larger by a factor of roughly 1.5 than those calculated in this research for the pure sample (7.837, 4.988 and 20.07 ppm/K for the *a*-axis, *c*-axis and volume, respectively). The most likely explanation for the difference in thermal expansion coefficients is the different methods used to synthesize hexacelsian.

4.2.4 Peak intensity issues

Large peak intensity mismatches were observed in the substituted samples, though not in the pure sample, as seen in Figure 4.17. In particular, the (00ℓ) peaks were overrepresented. Preferred orientation has previously been reported in X-ray powder diffraction of hexacelsian, due to the fact that it cleaves perfectly along the basal plane, i.e. (001) [57]. Therefore, the intensity mismatch was assumed to be due to preferred orientation. The refined March-Dollase preferred orientation factors of the (001) axis were 0.548(3) and 0.488(6) for the samples with approximately 7.5mol% MgO and 5mol% TiO_2, and with approximately 10mol% MgO and 6.67mol% TiO_2, respectively, for the X-ray diffraction data taken at 25ºC. The preferred orientation factor for the neutron diffraction data taken at 25ºC was 1.150(3) for the sample with 7.5mol% MgO and 5 mol% TiO_2. (Values equal to one indicate no preferred orientation. Values are less than one for flat plate sample holders, and greater than one for cylindrical sample holders.) As expected, the preferred orientation is greater in the X-ray diffraction data, which used a deep-well sample holder, than in the neutron diffraction data, which used a

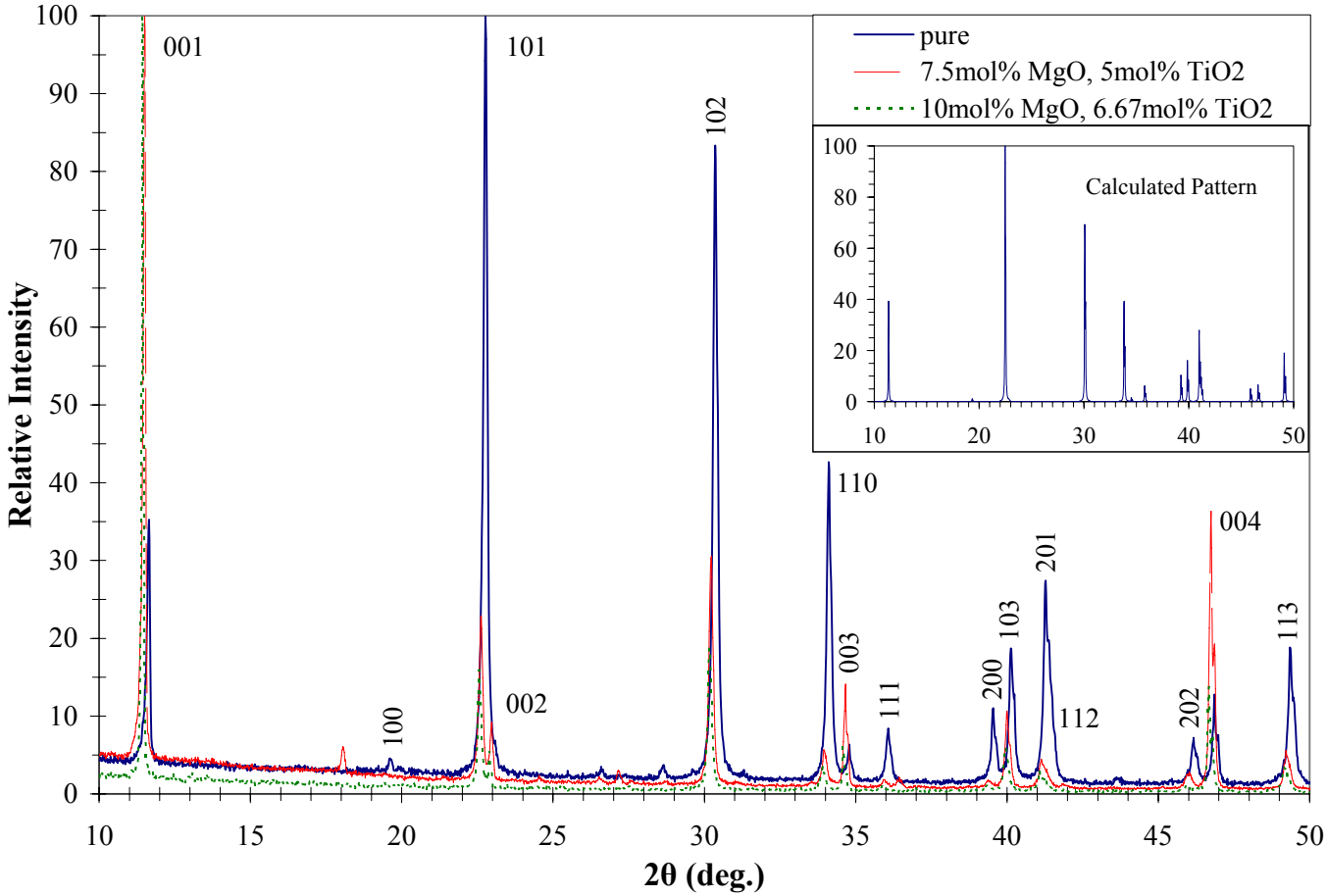

Figure 4.17 Diffraction patterns of hexacelsian with varying amounts of MgO and TiO_2 additions. The insert shows a calculated pattern for hexacelsian.

cylindrical sample can, due to the method for packing a powder sample into a deep-well sample holder.

In order to further investigate the peak intensity mismatches, two X-ray diffraction patterns were collected at room temperature on the sample with 10mol% MgO and 6.67mol% TiO_2; one utilized a deep-well sample holder, the other a side-load sample holder. The use of a side-load sample holder should negate the preferred orientation caused by packing the powder sample down into a deep-well sample holder. However, no large change in peak intensity mismatch was found, as seen in Figure 4.18, though the use of the side load sample holder did improve the peak intensity mismatch slightly. However, no improvement was seen in the (00ℓ) peak intensities. These findings suggest that preferred orientation is not the primary culprit for the peak intensity mismatch.

4.3 Structural Refinement

4.3.1 Pure hexacelsian sample

The pure hexacelsian structure was refined using both X-ray and neutron diffraction data. The starting structure, taken from Kremenović et al. [28], has the trigonal space group symmetry *P-3*. The lattice parameters were refined from the X-ray diffraction data. The refined lattice parameters for the pure hexacelsian sample are: *a*=5.2942(1) Å and *c*=7.7908(3) Å. The goodness of fit parameters were $\chi^2 = 5.257$, $R_{wp} = 0.0582$ and $R_{exp} = 0.0254$.

Due to the nature of neutron diffraction and difficulties in instrument alignment, the data is sensitive to zero errors, particularly time-of-flight neutron diffraction. Therefore, the lattice parameters determined from the X-ray data were imported into the neutron diffraction refinements, and were not further refined. The atomic parameters,

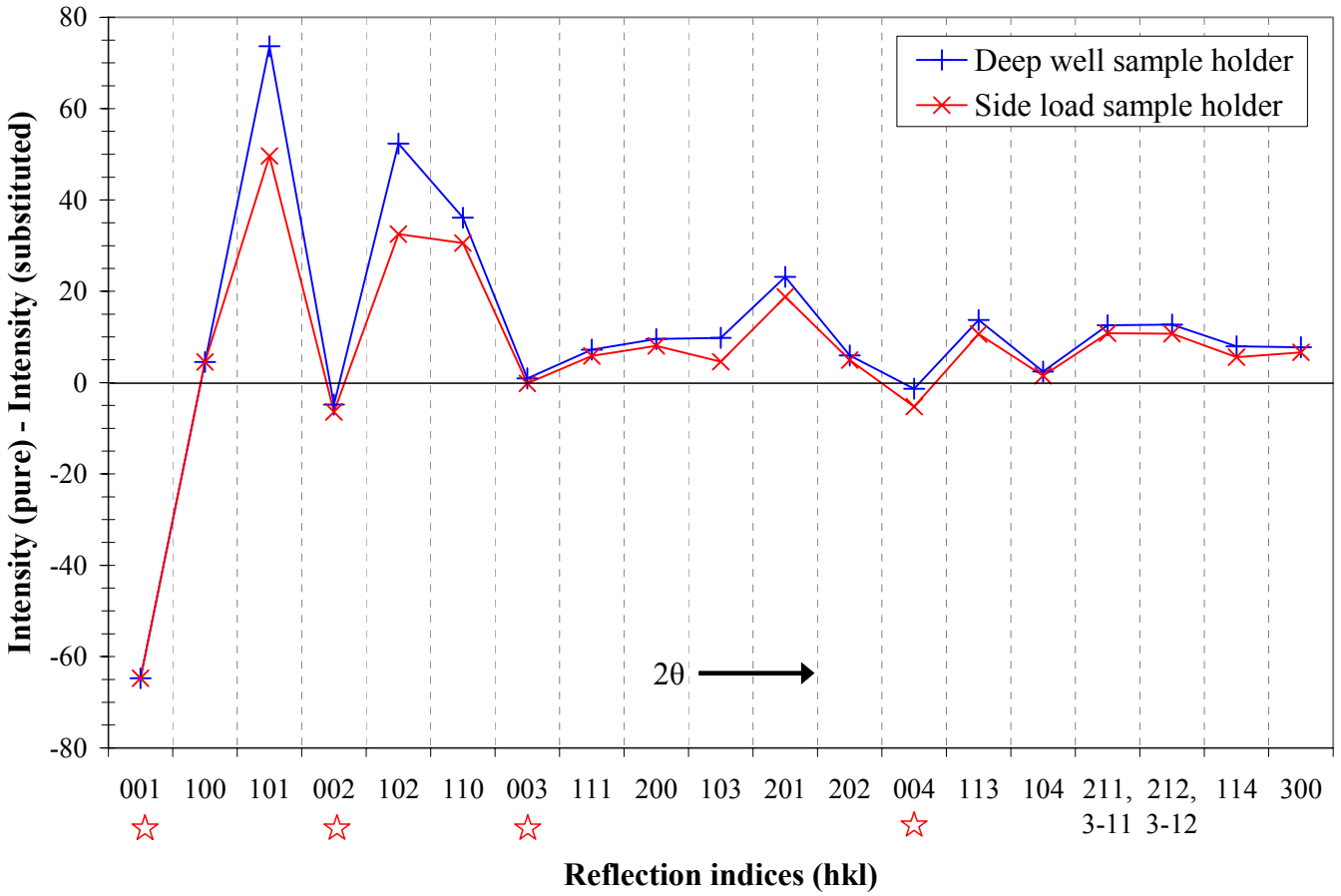

Figure 4.18 Difference in relative peak intensities between pure and 10mol% MgO, 6.67mol% TiO_2 samples using both deep-well and side-load sample holders. Red stars mark (00ℓ) peaks.

including site occupancies and thermal parameters, were refined from the neutron diffraction data of the pure sample. The refined structure is seen in Figure 4.19. Refinement of the site occupancies resulted in values of 1.0 for all atoms, indicating all sites were fully occupied. The refined atomic parameters are given in Table 4.2 below.

4.3.2 Refinement with doped cations

Neutron diffraction data of the sample with approximately 7.5mol% MgO and 5mol% TiO_2 were also refined. Initial refinements using the same *P-3* space group used for the X-ray diffraction data and not accounting for the substitutional cations gave a poor fit (χ^2 = 18.80,), which can not be explained by the substitutional cations alone. Refinement with a version of the trigonal *P-3* space group altered for Si/Al disorder improved the fit incrementally (χ^2 = 18.77). Refinements with the hexagonal *P6/mmm* and *$P6_3/mcm$* space groups, as reported by Ito [23] (*P6/mmm*) and Kremenović et al. [32] (*$P6_3/mcm$*), worsened the fit significantly (χ^2 = 77.56 and 84.95, respectively). The orthorhombic space groups *Immm*, *Pnam* and *$P2_1/a$* as well as the monoclinic space groups *C2/c* and *I12/c1* were unrefinable. None of the alternative structures tried improved the fit over the *P-3* space group.

Attempts were made to locate the Mg^{2+} and Ti^{4+} ions within the hexacelsian structure. A substitutional solid-solution was assumed. The substitutional cations were placed on various lattice sites, and the structure was refined to determine the effect on the goodness-of-fit parameters. The results are summarized in Table 4.3. The lattice sites were constrained to fully occupied, except where noted.

The barium cation radius is much larger than the magnesium and titanium cation radii, as can be seen in Table 4.4, which compares the ionic radii of the substitutional and lattice cations. The magnesium and titanium cation radii are larger than, but on the same order as, the aluminum and silicon radii. Therefore, it would be more favorable for the magnesium and titanium cations to substitute on the aluminum and silicon sites. Indeed,

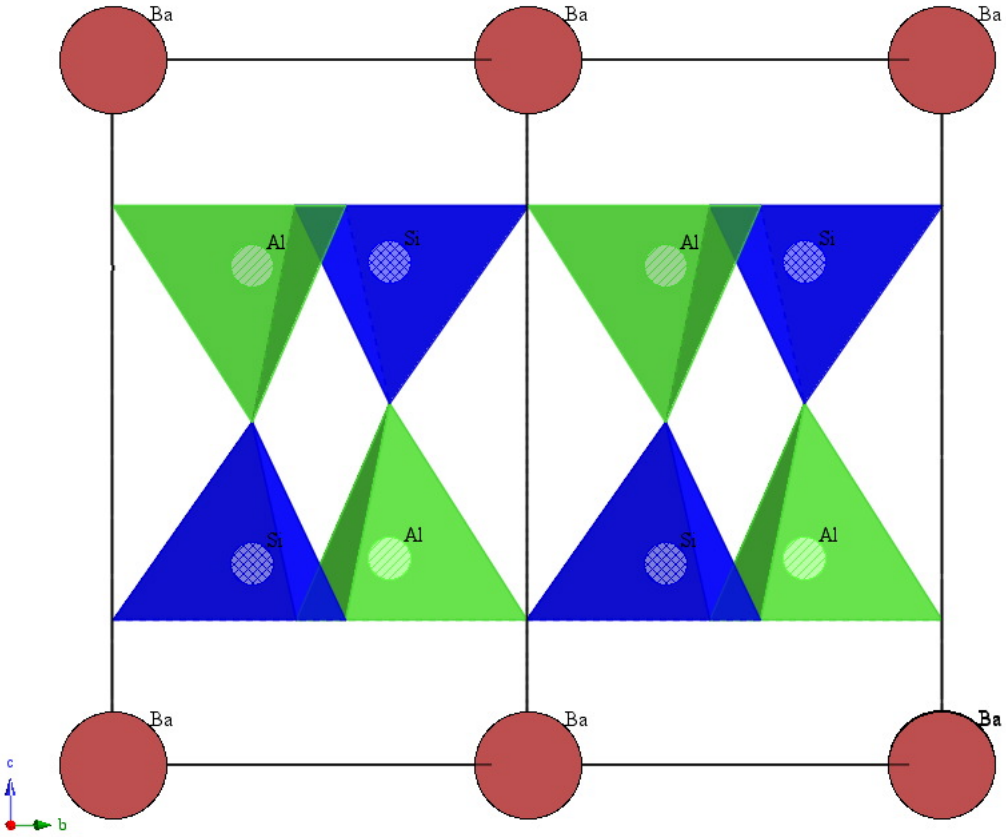

(a)

Figure 4.19 Refined *P-3* structure of pure hexacelsian. The solid red spheres represent barium ions, the aluminum-centered tetrahedra are green, with striped cations, and the silicon-centered tetrahedra are blue with cross-hatched cations. The crystal contains two unit cells in the *a*- and *b*-directions, and one unit cell in the *c*-direction. Part (a) is viewed along the *a*-axis. Part (b) is viewed along the *c*-axis.

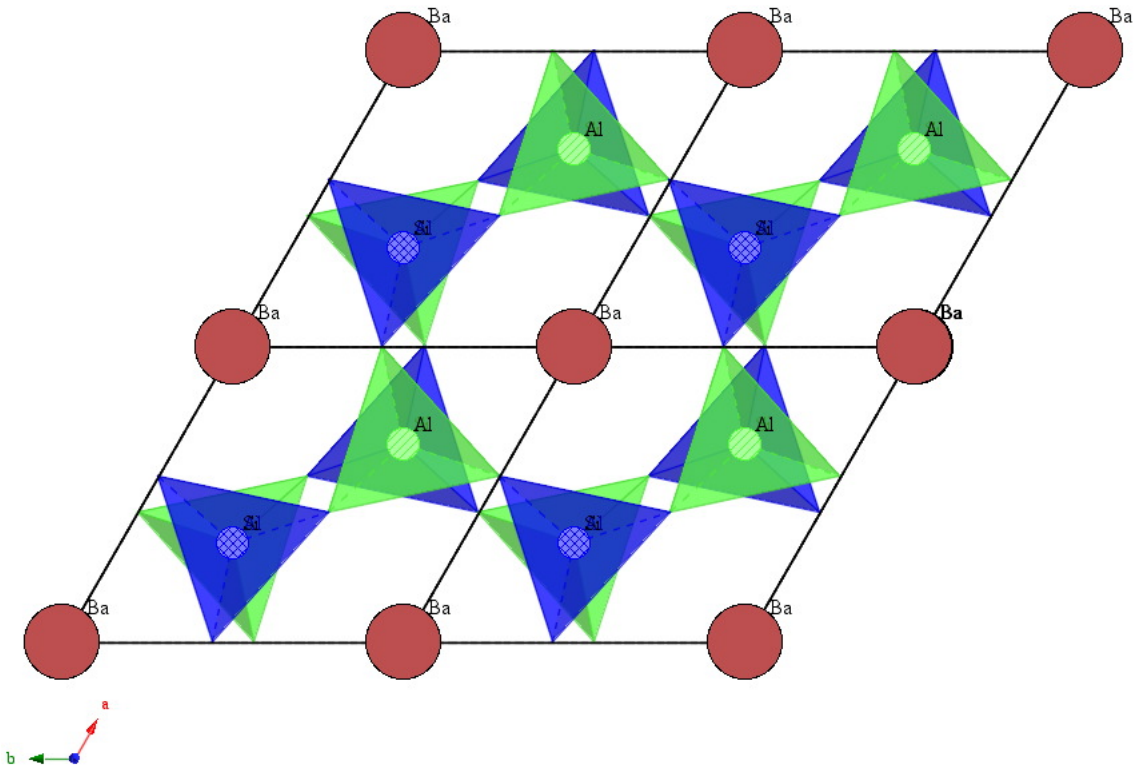

(b)

Figure 4.19 Continued.

Table 4.2 Refined atomic parameters for pure hexacelsian.

	Ba	**Si**	**Al**	**O1**	**O2**
x	0	0.3333	0.3333	0.3333	1.0007(6)
y	0	0.6667	0.6667	0.6667	0.4395(4)
z	0	0.7140(4)	0.2921(4)	0.5135(3)	0.2062(9)
$\mathbf{U_{iso}}$	0.0160(5)	0.0103(7)	0.0077(7)	--	--
$\mathbf{U_{11}}$	--	--	--	0.0176(4)	0.0103(4)
$\mathbf{U_{22}}$	--	--	--	0.0176(4)	0.040(1)
$\mathbf{U_{33}}$	--	--	--	0.0060(7)	0.0136(4)
$\mathbf{U_{12}}$	--	--	--	0.0088(2)	0.014(1)
$\mathbf{U_{13}}$	--	--	--	0	-0.0007(7)
$\mathbf{U_{23}}$	--	--	--	0	-0.0047(5)

Table 4.3 Substitution schemes investigated with refinement goodness-of-fit parameter.

Substitutional Ion (Occ.)	**Substitutional Site (Occ.)**	**Refined Occupancies**	χ^2
--	--	--	*18.80*
Ti (0.031(5))	Al (0.969(5))	--	18.73
Ti (0.037(5))	Si (0.963(5))	--	18.67
Mg (-0.1(1))	Ba (1.1(1))	--	18.80
Mg (-0.2(1))	Ba (1.2(1))	--	18.73
Ti (0.032(5))	Al (0.968(5))		
Ti (0.005(4))	Ba (0.995(4))	--	18.80
Mg (-0.23(3))	Si (1.23(3))	--	18.67
Mg (-0.11(2))	Al (1.11(2))	--	18.73
Mg (0.08(3))	Al (0.676)	Ba (1.08(3))	18.61
Ti (-0.302)		O1(1.06(2))	
		O2(1.09(3))	

Table 4.4 Cation radii of substitutional and lattice ions [59].

Cation	Radii (Å)	Coordination
Ba^{2+}	1.36	6
Al^{3+}	0.38	4
	0.53	6
Si^{4+}	0.29	4
	0.40	6
Mg^{2+}	0.49	4
	0.51	6
Ti^{4+}	0.44	6

it is found that placing the substitutional cations on the barium site does not improve the fit. However, none of the substitutional schemes improve the fit significantly. In addition, several of the schemes resulted in physically-impossible negative refined site occupancies and negative atomic displacement parameters.

The best fit (χ^2 = 18.61) was found with the last scheme in Table 4.3, in which Mg^{2+} and Ti^{4+} ions are placed on the aluminum site, and the barium and oxygen site fractions are refined. This scheme was based upon that proposed in a paper by Lee and Aswath [19]. They proposed that in hexacelsian with MgO additions, the Mg^{2+} ions would substitute on the Al^{3+} site with corresponding oxygen vacancies to balance the charge, according to equation (3) below. They also proposed that in hexacelsian with TiO_2 additions, the Ti^{4+} ions would also substitute on the Al^{3+} site with corresponding barium vacancies to balance the charge, according to equation (4) below.

$$2MgO_{BaAl2Si2O8} \rightarrow 2Mg^{\bullet}_{Al} + V^{\circ\circ}_{O} + 2O^{X}_{O} + V_{BaSi2O5} \quad (3)$$

$$2TiO_{2\ BaAl2Si2O8} \rightarrow 2Ti^{\circ}_{Al} + V^{\bullet\bullet}_{Ba} + 4O^{X}_{O} + 2V_{SiO2} \quad (4)$$

Lee and Aswath did not investigate the circumstance when both MgO and TiO_2 are present. Refinements of the neutron data with the substitutional schemes proposed by Lee and Aswath, though it resulted in the best goodness-of-fit parameter, had several problems. The Ti^{4+} refined to a negative site occupancy. Also, the barium and oxygen sites refined to occupancies greater than one, not less than one as would be expected for barium and oxygen vacancies.

5. CONCLUSIONS

5.1 MgO and TiO_2 Solubility in BAS

From the solid-state synthesis of the $BaAl_2Si_2O_8$ samples with MgO and TiO_2 additions, it may be inferred that Mg^{2+} and Ti^{4+} cations have limited solubility in BAS, as evidenced by the formation of a secondary phase, Mg_2TiO_4. Additions of 7.5mol% MgO and 5mol% TiO_2 were not able to go into solution at 1350ºC, even after extended heating for over 100 hours. Raising the temperature to 1620ºC allowed all but a trace of the Mg_2TiO_4 phase to dissolve into the primary BAS phase. Larger amounts of 10mol% MgO and 6.67mol% TiO_2 similarly caused the formation of large amounts of Mg_2TiO_4 at 1350ºC, which then decreased as the temperature increased. At 1635ºC, all but a trace of the Mg_2TiO_4 secondary phase dissolved into the primary phase.

However, increasing the amount of additions to 15mol% MgO and 10mol% TiO_2 resulted in the formation of a secondary Mg_2TiO_4 phase that could not be dissolved into solution, even after extended heating for over 200 hours in the 1440-1450ºC range. Further increases in temperature resulted in melting of the sample. These findings lead to several conclusions. First, the solubility of Mg^{2+} and Ti^{4+} into celsian at 1350ºC is less than 7.5mol% Mg^{2+} and 5mol% Ti^{4+}. At 1635ºC, their solubility is at least 10mol% Mg^{2+} and 6.67mol% Ti^{4+}. The solubility limit appears to be at a composition between 10mol% Mg^{2+}, 6.67mol% Ti^{4+} and 15mol% Mg^{2+}, 10mol% Ti^{4+}.

5.2 Mg^{2+} and Ti^{4+} Cation Locations within the Hexacelsian Structure

The substitutional Mg^{2+} and Ti^{4+} cations may be located on the aluminum lattice site, with corresponding barium and oxygen vacancies to balance the charge, similar to what was proposed by Lee and Aswath [19]. However, the substitutional cations were unable to be conclusively located due to a poor fit of the neutron diffraction data for the sample substituted with approximately 7.5mol% MgO and 5mol% TiO_2. The error in the fit comes primarily from two sources: peak intensity mismatch and extra peaks. The peak intensity mismatch, observed with both X-ray and neutron diffraction for the substituted samples, though not the pure sample, does not appear to be primarily due to preferred orientation. Use of a side-load sample holder did not alleviate the problem. The cause of the peak intensity mismatch is unknown.

Similarly for the extra peaks present, the cause is unclear. The peaks do not match the Mg_2TiO_4 secondary phase. The extra peaks also do not appear in the X-ray diffraction pattern. They are therefore most likely not due to a secondary phase. Discussions with the GPPD instrument scientist at IPNS ruled out the possibility of instrumental artifacts. The other possible explanation for extra peaks is the presence of a superlattice, particularly when substitutions and/or ordering are factors (as they are in this case). An oxygen superlattice might appear in neutron diffraction while not being observed in X-ray diffraction due to poor interaction of X-rays with light elements. However, the location of some of the extra peaks on the shoulders of hexacelsian peaks appears to rule out this possibility as well. The most likely explanation for both the peak intensity mismatch and extra peaks may be that the addition of Mg^{2+} and Ti^{4+} cations to hexacelsian significantly alters the structure in a way that has not been accounted for in the structural model thus far.

5.3 Effect of Synthesis Method

The thermal expansion coefficients of pure hexacelsian determined from high-temperature X-ray diffraction are less those previously reported by Kremenović et al. [12] for zeolite-derived hexacelsian (7.837, 4.988 and 20.07 ppm/K versus 10.5, 8.3 and 32 ppm/K for the *a*- and *c*- directions and the volume, respectively). On the other hand, the thermal expansion coefficients of the sample substituted with approximately 10mol% MgO and 6.67mol% TiO_2 (7.951, 5.024 and 20.97 ppm/K for the *a*- and *c*-directions and the volume) are similar to dilatometric thermal expansion coefficients previously reported for melt glass crystallized hexacelsian by Kohli [60] and Beall et al. [21]. Kohli reported a thermal expansion coefficient of 7.9 ppm/K for a hexacelsian sample with 20mol% MgO, 9mol% TiO_2 and 1mol% ZnO. Beall et al. reported thermal expansion coefficients of 7.8-8.4 ppm/K for hexacelsian samples with 20-29mol% MgO, 9mol% TiO_2 and 1mol% ZnO. Lower thermal expansion coefficients are generally desirable for applications [7].

In addition, the synthesis method appears to change the effect of substitutional cations on the α↔β transition. In the current research, using solid-state synthesis, additions up to 10mol% MgO and 6.67mol% TiO_2 were found to not suppress the α↔β phase transition, as evidenced by the non-stabilized thermal expansion (although the additions did depress the transition temperature). However, the patent by Beall et al. [21], using melt-glass crystallization synthesis, claims that additions of 5-25mol% MgO, 6-14mol% TiO_2, 0-10mol% ZnO, and 0-8mol% ZrO_2 should stabilize the thermal expansion and suppress the α↔β transition. It may be concluded that the method of synthesizing pure and substituted hexacelsian affects the thermal properties and phase relationships.

REFERENCES

1. Dittler, E. and H. Lasch, *New synthetic investigations in the feldspar group.* Ceramic Abstracts, 1932. **11**(11): p. 590-1.

2. Yoshiki, B. and K. Matsumoto, *High-temperature modification of barium feldspar*. Journal of the American Ceramic Society, 1951. **34**(9): p. 283-286.

3. Lin, H.C. and W.R. Foster, *Studies in the system BaO-Al2O3-SiO2 I. The polymorphism of celsian.* The American Mineralogist, 1968. **53**(1): p. 134-144.

4. Barthelmy, D., *Mineralogy Database*. 2004, http://webmineral.com.

5. Hall, F.P. and H. Insley, *Phase Diagrams for Ceramists*. 1947, American Ceramic Society.

6. Boškovic, S., et al., *Formation of celsian from mechanically activated BaCO3-Al2O3-SiO2 mixtures.* Journal of Alloys and Compounds, 1999. **290**(1-2): p. 230-235.

7. Kobayashi, Y., *Transformation kinetics from hexacelsian to celsian for powders having uniform particle size.* Ceramics International, 2001. **27**(2): p. 179-184.

8. Hoghooghi, B., et al., *Synthesis of Celsian Ceramics from Zeolite Precursors.* Journal of Non-Crystalline Solids, 1994. **170**(3): p. 303-307.

9. Lee, K.T. and P.B. Aswath, *Enhanced production of celsian barium aluminosilicates by a three-step firing technique.* Materials Chemistry and Physics, 2001. **71**(1): p. 47-52.

10. Drummond, C.H., III and N.P. Bansal. *Crystallization behavior and properties of BaO*Al2O3*2SiO2 glass matrices*. in *Ceramic Engineering and Science*. 1990: American Ceramic Society.

11. Beall, G.H., *Refractory glass-ceramics*, in *High Temperature Oxides Part IV: Refractory Glasses, Glass-Ceramics, and Ceramics*, A.M. Alper, Editor. 1971, Academic Press: New York. p. 15-36.

12. Kremenovic, A., et al., *High-temperature synchrotron powder diffraction investigation of thermal expansion, strain and microstructure for the co-elastic alpha <->beta hexacelsian transition.* Phase Transitions, 1999. **68**(4): p. 587-605.

13. Sung, Y.M. and J.W. Ahn, *Sintering and crystallization of off-stoichiometric BaO center dot Al2O3 center dot 2SiO2 glasses.* Journal of Materials Science, 2000. **35**(19): p. 4913-4918.

14. Quander, S.W., A. Bandyopadhyay, and P.B. Aswath, *Synthesis and properties of in situ Si3N4-reinforced BaO center dot Al2O3 center dot 2SiO(2) ceramic matrix composites.* Journal of Materials Science, 1997. **32**(8): p. 2021-2029.

15. Lansmann, V. and M. Jansen, *Application of the glass-ceramic process for the fabrication of whisker reinforced celsian-composites.* Journal of Materials Science, 2001. **36**(6): p. 1531-1538.

16. Drummond, C.H., III, et al. *Crystallization of a barium-aluminosilicate glass*. in *Ceramic Engineering and Science*. 1989: American Ceramic Society.

17. Bahat, D., *Kinetic Study of Hexacelsian-Celsian Phase Transformation.* Journal of Materials Science, 1970. **5**(9): p. 805-&.

18. Bahat, D., *Homogenous and heterogeneous polymorphic transformations in alkaline earth feldspars.* Journal of Materials Science, 1978. **13**(12): p. 2548-2554.

19. Lee, K.T. and P.B. Aswath, *Role of mineralizers on the hexacelsian to celsian transformation in the barium aluminosilicate (BAS) system.* Materials Science and Engineering a-Structural Materials Properties Microstructure and Processing, 2003. **352**(1-2): p. 1-7.

20. Hyatt, M.J. and N.P. Bansal, *Crystal growth kinetics in BaOAl(2)O(3)2SiO(2) and SrOAl(2)O(3)2SiO(2) glasses.* Journal of Materials Science, 1996. **31**(1): p. 172-184.

21. Beall, G.H., H.J. Holland, and J.T. Kohli, *Glass-ceramic containing a stabilized hexacelsian crystal structure*. 1999, Corning Incorporated: United States.

22. Rawn, C.J., et al., *Neutron powder diffraction studies of hexacelsian with and without MgO and TiO_2 additions*, Oak Ridge National Laboratory: Oak Ridge, TN.

23. Ito, T., *Alpha-Celsian*, in *X-ray studies on polymorphism*. 1950, Maruzen: Tokyo. p. 19-29.

24. Withers, R.L., et al., *The inherent displacive flexibility of the hexacelsian tetrahedral framework and its relationship to polymorphism in Ba-hexacelsian.* Physics and Chemistry of Minerals, 2000. **27**(10): p. 747-756.

25. Takéuchi, Y., *A detailed investigation of the structure of hexagonal $BaAl_2Si_2O_8$ with reference to its α–β inversion.* Mineralogical Journal, 1958. **2**(5): p. 311-332.

26. Müller, W.F., *Phase-transitions and associated domains in hexacelsian (BaAl2Si2O8).* Physics and Chemistry of Minerals, 1977. **1**(1): p. 71-82.

27. Xu, Z.K., J.L. Shull, Jr., and W.M. Kriven, *Hot-stage transmission electron microscopy study of phase transformations in hexacelsian (BaAl2Si2O8).* Journal of Materials Research, 2002. **17**(6): p. 1287-1297.

28. Kremenovic, A., et al., *Time-temperature resolved synchrotron XRPD study of the hexacelsian alpha <->beta polymorph inversion.* Solid State Ionics, 1997. **101**: p. 611-618.

29. Tabira, Y., et al., *Structured diffuse scattering, displacive flexibility and polymorphism in Ba-hexacelsian.* Physics and Chemistry of Minerals, 2000. **27**(3): p. 194-202.

30. Colomban, P., et al., *Sol-gel-prepared pure and lithium-doped hexacelsian polymorphs: An infrared, Raman, and thermal expansion study of the beta-phase stabilization by frozen short-range disorder.* Journal of the American Ceramic Society, 2000. **83**(12): p. 2974-2982.

31. Dove, M.T., *Structure and Dynamics: An atomic view of materials*. 1 ed. Oxford Master Series in Condensed Matter Physics. 2003, New York: Oxford University Press. 334.

32. Kremenovic, A., et al., *Structural and spectroscopic characterization of the quenched hexacelsian.* Journal of Physics and Chemistry of Solids, 2003. **64**(11): p. 2253-2268.

33. Lee, K.-T. and P.B. Aswath, *Synthesis of hexacelsian barium aluminosilicate by a solid-state process.* Journal of the American Ceramic Society, 2000. **83**(12): p. 2907-2912.

34. Okada, K., et al., *Uptake of various cations by amorphous BaAl2Si2O8 prepared by solid-state reaction of kaolin with BaCO3.* Materials Letters, 2003. **57**(22-23): p. 3554-3559.

35. Fu, Y.P., et al., *Solid-state synthesis of ceramics in the BaO-SrO-Al2O3-SiO2 system.* Ceramics International, 2004. **30**(1): p. 41-45.

36. Bansal, N.P. and M.J. Hyatt, *Crystallization kinetics of Bao-Al2O3-SiO2 glasses.* Journal of Materials Research, 1989. **4**(5): p. 1257-1265.

37. Chen, M., W.E. Lee, and P.F. James, *Preparation and characterization of alkoxide-derived celsian glass-ceramic.* Journal of Non-Crystalline Solids, 1991. **130**(3): p. 322-325.

38. Debsikdar, J.C., *Gel to glass conversion and crystallization of alkoxy-derived barium aluminosilicate gel.* Journal of Non-Crystalline Solids, 1992. **144**(2-3): p. 269-276.

39. Lee, W.E., M.K. Chen, and P.E. James, *Crystallization of celsian (BaAl2Si2O8) glass.* Journal of the American Ceramic Society, 1995. **78**(8): p. 2180-2186.

40. Liu, C.L., S. Komarneni, and R. Roy, *Crystallization and seeding effect in BaAl2Si2O8 gels.* Journal of the American Ceramic Society, 1995. **78**(9): p. 2521-2526.

41. McKittrick, J., B. Hoghooghi, and O.A. Lopez, *Vitrification and crystallization of barium aluminosilicate glass ceramics from zeolite precursors.* Journal of Non-Crystalline Solids, 1996. **197**(2-3): p. 170-178.

42. Dell'Agli, G., et al., *Thermal transformation of Ba-exchanged A and X zeolites into monoclinic celsian.* Solid State Ionics, 2000. **127**(3-4): p. 309-317.

43. Djordjevic, J., et al., *Structural investigations of celsian glass derived from Ba-LTA zeolite.* Physical Chemistry Chemical Physics, 2001. **3**(8): p. 1560-1565.

44. Aronne, A., et al., *FTIR study of the thermal transformation of barium-exchanged zeolite A to celsian.* Journal of Materials Chemistry, 2002. **12**(10): p. 3039-3045.

45. Ferone, C., et al., *New insight into the thermal transformation of barium-exchanged zeolite A to celsian.* Chemistry of Materials, 2002. **14**(2): p. 797-803.

46. Zhang, X.D., K.H. Sandhage, and H.L. Fraser, *Synthesis of BaAl2Si2O8 from solid Ba-Al-Al2O3-SiO2 precursors: II, TEM analyses of phase evolution.* Journal of the American Ceramic Society, 1998. **81**(11): p. 2983-2997.

47. Schmutzler, H.J. and K.H. Sandhage, *Transformation of Ba-Al-Si precursors to celsian by high-temperature oxidation and annealing.* Metallurgical and Materials Transactions B-Process Metallurgy and Materials Processing Science, 1995. **26**(1): p. 135-148.

48. Colella, C. and R. Aiello, *Thermal conversion of synthetic cymrite into hexagonal barium feldspar.* Thermochimica Acta, 1978. **27**(1-3): p. 253-&.

49. Winter, W., *Characterization of BaO-Al2O3-SiO2 (BAS) gels during heat treatment.* Journal of Materials Science, 1996. **31**(12): p. 3087-3094.

50. Müller, U., *Inorganic Structural Chemistry*. Inorganic Chemistry: A Textbook Series, ed. G. Meyer and A. Nakamura. 1993, New York: John Wiley & Sons. 264.

51. Corbin, D.R., et al. *Designing zeolites as novel precursors to electronic ceramics*. in *Synthesis/characterization and novel applications of molecular sieve materials*. 1991. Anaheim, California, USA: Materials Research Soc.

52. Kirkham, M.J., S.A. Speakman, and C.J. Rawn. *Quantification of the consequences of using parallel-beam optics combined with linear position sensitive detectors*. in *Advances in X-ray Analysis, vol. 47: Proceedings of the 52nd Annual Denver X-ray Conference*. 2003. Denver, Colorado.

53. Sears, V.F., *Neutron scattering lengths and cross-sections.* Neutron News, 1992. **3**(3): p. 26-27.

54. Rietveld, H.M., *A profile refinement method for nuclear and magnetic structures.* Journal of Applied Crystallography, 1969. **2**(2): p. 65-71.

55. Larson, A.C. and R.B. Von Dreele, *General Structure Analysis System*. 1994, Los Alamos National Laboratory Report LAUR 86-748.

56. Toby, B.H., *EXPGUI, a graphical user interface for GSAS.* Journal of Applied Crystallography, 2001. **34**: p. 210-213.

57. Villar, M.C.G. and C.G. Monzonis, *Determination of hexacelsian by infrared-spectroscopy.* Talanta, 1984. **31**(7): p. 550-552.

58. Callister, W.D., Jr., *Materials Science and Engineering: An Introduction*. Fifth ed. 2000, New York: John Wiley & Sons, Inc. 661-662.

59. Shannon, R.D., *Revised Effective Ionic-Radii and Systematic Studies of Interatomic Distances in Halides and Chalcogenides.* Acta Crystallographica Section A, 1976. **32**(SEP1): p. 751-767.

60. Kohli, J.T., *Glass ceramic rear panel for emissive display*. 1998, Corning Incorporated: United States.

APPENDIX

Table A.1 Compositions of pure (P), 15mol% MgO (C), 10mol% TiO_2 (D) samples.

Target Composition MgO-TiO_2 (mol%)	**Sample Name**	**$BaCO_3$**		**Al_2O_3**		**SiO_2**		**MgO**		**TiO_2**	
		g	mol%	g	mol%	g	mol%	g	mol%	g	mol%
0-0	P1	1.5763	24.99	0.8150	25.01	0.9603	50.00	--	--	--	--
	P2	1.5763	24.99	0.8146	25.00	0.9603	50.01	--	--	--	--
	P3	1.0511	25.00	0.5431	25.00	0.6399	49.99	--	--	--	--
	P4	1.0515	25.00	0.5433	25.00	0.6402	50.00	--	--	--	--
15-0	C1	1.4657	21.22	0.7572	21.22	0.8922	42.42	0.2137	15.15	--	--
	C2	1.4660	21.25	0.7572	21.25	0.8924	42.49	0.2115	15.01	--	--
0-10	D1	2.8810	22.50	1.4886	22.50	1.7545	45.00	--	--	0.5184	9.999

Table A.2 Compositions of all samples substituted with MgO and TiO_2.

Target Composition MgO-TiO_2 (mol%)	**Sample Name**	**$BaCO_3$**		**Al_2O_3**		**SiO_2**		**MgO**		**TiO_2**	
		g	mol%	g	mol%	g	mol%	g	mol%	g	mol%
15-10	A1	1.3143	18.75	0.6792	18.75	0.8004	37.49	0.2149	15.01	0.2840	10.00
	A2	1.3145	18.74	0.6792	18.74	0.8005	37.49	0.2151	15.02	0.2841	10.01
	A3	0.8769	18.76	0.4534	18.77	0.5337	37.50	0.1427	14.95	0.1895	10.01
	A4	0.8762	18.73	0.4525	18.73	0.5342	37.51	0.1435	15.02	0.1895	10.01
	A5	2.6294	18.75	1.3585	18.75	1.6013	37.50	0.4297	15.00	0.5679	10.00
	A7	2.6293	18.75	1.3585	18.75	1.6014	37.50	0.4279	15.00	0.5679	10.00
	A9*	2.6293	23.26*	1.3294	22.77*	1.6012	46.53*	0.1031	4.466*	0.1361	2.974*
10-6.67	F1	2.8166	20.83	1.4552	20.83	1.7153	41.67	0.2761	10.00	0.3652	6.671
7.5-5	B1	1.4525	21.87	0.7506	21.88	0.8846	43.75	0.1017	7.498	0.1344	4.999
	B2	1.4524	21.87	0.7507	21.88	0.8846	43.75	0.1016	7.490	0.1345	5.003
5-3	E1	3.0001	23.00	1.5503	23.00	1.8269	46.00	0.1333	5.002	0.1586	3.003

* Amounts in mole percents are incorrect due to BaO, Al_2O_3 and SiO_2 loss before MgO and TiO_2 addition.

Table A.3 Heating schedules for pure (P), 15mol% MgO (C), 10mol% TiO2 (D) samples.

P1/2		P3/4		P sol-gel*		C1/2		D1/2	
Temp. °C	**Time h**	**Temp. °C**	**Time h**	**Temp. °C**	**Time h**	**Temp. °C**	**Time h**	**Temp. °C**	**Time h**
800	4	800	20	600	24	800	23	850	24
1200	24	1350	24	800	24	1000	23	1100	24
1200	24	1600	18			1200	24	1350	93
1350	24	1650	24			1350	24		
1500	24					1350	24		
1600	24								

* Synthesized using the sol-gel method. All others by solid-state method.

Table A.4 Heating schedules for samples with 15mol%MgO and 10mol%TiO_2.

A1/2		A3/4		A5		A7		A9	
Temp. °C	**Time h**	**Temp. °C**	**Time h**	**Temp. °C**	**Time h**	**Temp. °C**	**Time h**	**Temp. °C**	**Time h**
800	23	800	24	850	24	850	48	1150	4
1350	23	1000	24	1000	24	1000	24	1200	6
1650*	24	1100	24	1100	24	1200	48	1200	2
		1200	24	1200	24	1400	48	1200	4
		1350	24	1300	24	1410	12		
		1500*	24	1350	24	1420	12		
				1400	24	1430	12		
				1440	24	1440	12		
				1460†	24	1440	12		
						1450	12		
						1440	24		
						1450	24		
						1440	24		
						1450	24		
						1440	24		
						1440	24		
						1450	24		
						1450	12		
						1460	12		
						1650*	48		
						1000	4		
						1000	4		
						1100	4		
						1100	5		

* Sample melted. † Sample fused to alumina boat.

Table A.5 Heating schedules for other samples with MgO and TiO_2.

F1		B1/2		E1	
Temp. °C	**Time h**	**Temp. °C**	**Time h**	**Temp. °C**	**Time h**
850	24	850	24	800	24
1000	24	1100	24	1100	24
1100	24	1350	24	1350	24
1200	24	1350	24	1500	24
1300	24	1350	24	1650*	24
1350	24	1350	60		
1400	24	1370	24		
1440	24	1385	24		
1460	24	1400	24		
1470	48	1410	4		
1480	48	1420	16		
1490	60	1430	22		
1500	24	1440	24		
1515	24	1450	24		
1520	24	1460	23		
1520	88.5	1470	24		
1530	24	1480	4		
1540	24	1490	17		
1550	48	1500	5		
1560	24	1510	24		
1570	24	1520	4		
1585	24	1550	18.5		
1600	72	1570	4.75		
1620	24	1585	17		
1635	24	1600	22		
		1620	24		
		1650	24		

* Sample melted.

VITA

Melanie Jean Kirkham graduated from Hendersonville High School in Hendersonville, Tennessee in 1998. She received a B.S. in Materials Science and Engineering in 2002, and an M.S., also in Materials Science and Engineering, in 2005 from the University of Tennessee, Knoxville.